



5-1991

## **Analysis of wind velocity calculations from measurements made from an ascending meteorological rocket**

Terry S. Paige

Follow this and additional works at: [https://trace.tennessee.edu/utk\\_gradthes](https://trace.tennessee.edu/utk_gradthes)

---

### **Recommended Citation**

Paige, Terry S., "Analysis of wind velocity calculations from measurements made from an ascending meteorological rocket. " Master's Thesis, University of Tennessee, 1991.  
[https://trace.tennessee.edu/utk\\_gradthes/12497](https://trace.tennessee.edu/utk_gradthes/12497)

This Thesis is brought to you for free and open access by the Graduate School at TRACE: Tennessee Research and Creative Exchange. It has been accepted for inclusion in Masters Theses by an authorized administrator of TRACE: Tennessee Research and Creative Exchange. For more information, please contact [trace@utk.edu](mailto:trace@utk.edu).

To the Graduate Council:

I am submitting herewith a thesis written by Terry S. Paige entitled "Analysis of wind velocity calculations from measurements made from an ascending meteorological rocket." I have examined the final electronic copy of this thesis for form and content and recommend that it be accepted in partial fulfillment of the requirements for the degree of Master of Science, with a major in Mechanical Engineering.

Frank G. Collins, Major Professor

We have read this thesis and recommend its acceptance:

Ralph D. Kimberlin, Charlues Paludan

Accepted for the Council:

Carolyn R. Hodges

Vice Provost and Dean of the Graduate School

(Original signatures are on file with official student records.)

To the Graduate Council:

I am submitting herewith a thesis written by Terry S. Paige, entitled "Analysis of Wind Vector Calculations from Measurements Made from an Ascending Meteorological Rocket." I have examined the final copy of this thesis for form and content and recommend that it be accepted in partial fulfillment of the requirements for the degree of Master of Science, with a major in Mechanical Engineering.

*Frank G. Collins*

Frank G. Collins, Major Professor

We have read this thesis  
and recommend its acceptance:

*Ralph D. Kimberlin*

*Charles J. N. Saludan*

*Edward M. Craft*

Accepted for the Council:

*Cowminkel*

Vice Provost  
and Dean of The Graduate School

ANALYSIS OF WIND VELOCITY CALCULATIONS FROM MEASUREMENTS  
MADE FROM AN ASCENDING METEOROLOGICAL ROCKET

A Thesis

Presented for the

Master of Science

Degree

The University of Tennessee, Knoxville

Terry S. Paige

May 1991

## ACKNOWLEDGMENTS

The author expresses his thanks to personnel at FWG Associates, Inc., National Aeronautics and Space Administration (NASA) Marshall Space Flight Center, San Jose State University, NASA Ames Research Center, NASA Dryden Flight Research Center, Orbital Science Corporation, Arnold Engineering Development Center, National Center for Atmospheric Research, Rosemount, Inc., the University of Wyoming, the University of North Dakota, and the University of Tennessee Space Institute, for material, sources, advice, and text and figure preparation. The author also thanks his thesis committee, Frank Collins, Ted Paludan, Ed Kraft, and Ralph Kimberlin, for their guidance and their toleration of the ignorance and impatience of their student.

This thesis was made possible in part with funding from FWG Associates, Inc., under contract to NASA Marshall Space Flight Center, the support of the author's wife, and early bedtimes for small children.

## ABSTRACT

The feasibility of using a meteorological rocket as a platform for measurements pertinent to wind velocity calculations is determined. The equations for wind velocity calculations from measurements taken from an airborne platform are developed along with an uncertainty analysis. Commercially available instrumentation is analyzed for use on the rocket propelled platform with the resulting wind velocity calculation uncertainty quantified.

## TABLE OF CONTENTS

CHAPTER	PAGE
I. INTRODUCTION . . . . .	1
II. WIND VELOCITY CALCULATIONS FROM AN AIRBORNE PLATFORM . . . . .	6
Air Velocity . . . . .	7
Rotation Transformation . . . . .	11
Velocity Transformation . . . . .	12
Summary . . . . .	12
III. MEASUREMENTS AND INSTRUMENTATION . . . . .	14
Airspeed . . . . .	15
Flow Angle . . . . .	18
Rocket Inertial Motion . . . . .	22
Data Sampling . . . . .	25
IV. UNCERTAINTY ANALYSIS . . . . .	26
V. ROCKET PERFORMANCE . . . . .	33
Existing Design . . . . .	33
New Design . . . . .	35
V. INSTRUMENTATION SPECIFICATION AND WIND VELOCITY UNCERTAINTY . . . . .	39
Maximum Measurement Uncertainty for Design . . . . .	40
Pressure and Temperature Measurement Feasibility . . . . .	42
Inertial Attitude Measurement Feasibility . . . . .	43
Acceleration Measurement Feasibility . . . . .	43
Flow Angle Measurement Feasibility . . . . .	44
Rocket and Measurement Specifications . . . . .	45

VII. CONCLUSIONS . . . . .	47
LIST OF REFERENCES . . . . .	49
APPENDIX . . . . .	53
VITA . . . . .	57



## LIST OF FIGURES

FIGURE	PAGE
1.0 Rocket and Dart Concept . . . . .	4
2.1 Body-fixed and Vehicle-centered Coordinate Frames and Euler Angles . . . . .	8
2.2 Angle-of-Attack and Sideslip Angle Definitions [17]. . . . .	10
2.3 Air Velocity Decomposition . . . . .	10
3.1 Effects of Mach Number and Yaw on the Reading of a Static Tube at $l/d = 3$ (Adapted from Howarth, et al. [8]) . . . . .	16
3.2 Recovery Factor for a Pratt and Whitney Total Temperature Probe (Adapted from Volluz [9]) . . . . .	17
3.3 Free Vanes on an Air Data Probe for Angle Measurements [31] . . . . .	19
3.4 ER-2 Radome with Angle-of-Attack and Sideslip Angle Pressure Ports [15] . . . . .	19
3.5 Conrad, Conical, and Hemispherical Flow Angle Probes . . . . .	20
4.1 Wind Vector Uncertainty from Body-fixed Wind Vector Uncertainty, Acceleration Measurement Uncertainty, Euler Angle Uncertainty, and Airspeed . . . . .	28
4.2 Body-fixed Wind Velocity Uncertainty from Airspeed and Flow Angle Uncertainties . . . . .	29
4.3 Calculated Airspeed Uncertainty from Pressure and Temperature Measurement Uncertainties . . . . .	32
5.1 Super Loki and New Design Predicted Mach Number with a 30-pound, 3-inch Diameter Dart . . . . .	34
5.2 Predicted Total Pressure for a 30-pound, 3-inch Diameter Dart . . . . .	37
5.3 Predicted Total Temperature for a 30-pound, 3-inch Diameter Dart . . . . .	38

A.1 Decomposition of a Rotating Coordinate Axis into Fixed and Rotating  
Components . . . . . 56

## NOMENCLATURE

- $\vec{a}_{BF}$  Body-fixed acceleration
- $a_x$  Acceleration component in the  $x$  direction
- $a_y$  Acceleration component in the  $y$  direction
- $a_z$  Acceleration component in the  $z$  direction
- $d$  Probe diameter
- $F$  An arbitrary function
- $\vec{F}$  A fixed vector
- $k$  Flow angle sensitivity factor
- $L_{BV}$  Vehicle-centered to body-fixed frame vector transformation matrix
- $l$  Shoulder to orifice probe length
- $l_x$  Displacement component of the gust probe in the  $x$  direction
- $l_y$  Displacement component of the gust probe in the  $y$  direction
- $l_z$  Displacement component of the gust probe in the  $z$  direction
- $M$  Mach number
- $p$  Roll rate
- $p_m$  Measured pressure
- $p_s$  Static pressure
- $p_t$  Total pressure
- $p_\infty$  Static pressure
- $q$  Dynamic pressure
- $r$  Yaw rate
- $r$  Total temperature probe recovery factor
- $R$  Ideal gas constant for air
- $\vec{R}$  A rotating vector
- $\vec{R}'$  A vector after rotation
- $T_o$  Total temperature
- $T_m$  Measured temperature
- $T_\infty$  Static temperature
- $t$  Time
- $t_o$  Initial time
- $\vec{V}$  An arbitrary vector
- $V_a$  Airspeed
- $\vec{V}_{GS}$  Vehicle inertial velocity
- $\vec{W}_{BF}$  Body-fixed air velocity
- $\vec{W}_{VC}$  Vehicle-centered air Velocity
- $\vec{W}$  Earth-surface wind velocity
- $\vec{x}_i$  A body-fixed frame coordinate axis
- $\vec{x}'_i$  A body-fixed frame coordinate axis
- $x_i$  A component of a body-fixed frame coordinate axis

- $\alpha$  Angle-of-attack
- $\beta$  Angle-of-sideslip
- $\gamma$  Ratio of specific heats
- $\Delta()$  Uncertainty of the parameter in ()
- $\Delta()$  A finite change of the parameter in ()
- $\tau$  Integration dummy variable
- $\xi_i$  A set of independent variables
- $\phi$  Bank angle
- $\psi$  Heading
- $\theta$  Elevation angle
- $\theta$  Displacement angle
- $\vec{\omega}$  Body-fixed rotation rate vector
- $\omega$  Rotation rate magnitude

# Chapter I

## Introduction

This thesis documents a feasibility investigation of using a meteorological rocket as an instrumentation platform for measurements pertinent to wind velocity calculations in support of space shuttle launches. Most of the work reported herein has been previously reported by Paige, et al. [1]. Prior to space shuttle launches, the wind profile along the shuttle ascent path must be known for evaluation of aerodynamic loading on the shuttle from the wind and wind-shears. The wind data is used in a shuttle ascent digital simulation for prediction of the shuttle response to these winds. Should the predicted response of the shuttle exceed pre-designated structural and control margins, the launch of the shuttle is delayed or canceled for that day.

Presently, balloons are released and tracked by radar for wind measurement. The balloons, known as Jimspheres, are assumed to have a zero slip velocity with the horizontal wind. Thus, the horizontal velocity vector of the Jimsphere, calculated by differentiation of the position of the Jimsphere as determined by radar, is assumed to be the velocity vector of the wind at the altitude of the Jimsphere.

The Jimsphere has a published accuracy of 0.5 m/s [2] and provides the information for wind calculations up to 60 kft. Drawbacks of the Jimsphere/radar system for measuring winds aloft include the long data acquisition time necessary to obtain prelaunch data and Jimsphere drift from the anticipated shuttle ascent path in high winds. Both of these drawbacks are consequences of the slow ascent rate of the Jimsphere (5 m/s). Typically, a balloon requires slightly more than one hour to rise to its maximum altitude of 55-60 kft above sea level (ASL), where it subsequently explodes. A minimum lead time of two hours is presently required

before shuttle launch for the last pre-launch Jimsphere release. After the first hour, during which the Jimsphere rises to altitude, the radar time, azimuth, elevation, and range (TAER) data is sent from Cape Canaveral, where it is reduced to wind magnitude and direction data filtered over altitude intervals of 100 ft, to Johnson Space Center. This calculated wind data is then used by a shuttle "loads code" which predicts the behavior of the ascending shuttle due to the aerodynamic loads produced by the winds aloft.

Because of the lead time between the wind measurements and the shuttle launch, the uncertainty in the wind profile at launch time is greater than the uncertainty which would otherwise be incurred by measurements made temporally closer to launch. This increased uncertainty further restricts the shuttle ascent safety margins and could cause an unnecessary launch delay, or as suggested by some researchers, a catastrophe [3].

The potential additional costs associated with unnecessary launch delays due to the present uncertainty in winds aloft predictions prompted a feasibility study of using an airplane as a platform for measurements pertinent to wind velocity calculations. Because an airplane can climb to 60 kft ASL in a relatively short time, the delay between the acquisition of the data used in the wind vector calculation and the shuttle launch would be decreased significantly, thus potentially providing a more accurate wind profile.

The use of an airplane as a platform for wind profile measurement is a proven technique for providing wind profiles comparable in accuracy to wind profiles measured by Jimspheres within established margins [4]. However, due to the operational cost of an airplane [5], the use of an airplane for shuttle launch support was rejected. Thus, the use of a meteorological rocket as an instrumentation platform

for measurements similar to those that have been successfully made from airplanes is considered herein.

A rocket is a desirable alternative to either a Jimsphere or an airplane for several reasons: 1) a rocket can measure winds more closely to the shuttle ascent path than either the airplane or a Jimsphere, and 2) a rocket can collect the data necessary for wind vector calculations more quickly (in one minute) than an airplane (which requires 15 minutes or less) and significantly more quickly than a Jimsphere (which requires one hour), expediting the shuttle loading evaluation. A rocket also has the potential advantages of low production and operational costs and independence from radar support.

The rocket and instrumentation pallet concept is illustrated in Figure 1. A dart, containing the instrumentation and data acquisition and telemetry hardware, would be propelled by a small rocket. An air data probe, extending forward from the dart, would be used for measurement necessary for air velocity calculations. Internal to the dart would be transducers measuring different aspects of the rocket dynamics. The pertinence of the air velocity calculations and dart dynamics measurements to the wind velocity calculations will be discussed further in Sections 2 and 3. The data acquisition and telemetry hardware, although necessary system components, will not be discussed herein.

This thesis begins by reviewing the process by which winds aloft are calculated using measurements made from an airborne platform. In doing so, the necessary measurements required to support those calculations will be defined. Instrumentation on two airplanes currently used for wind measurements, an F-104 airplane based at Dryden Flight Research Center and an ER-2 airplane based at Ames Research Center, will be considered for use on the rocket based instrumentation pallet. Although numerous other airplanes have been used for the determination

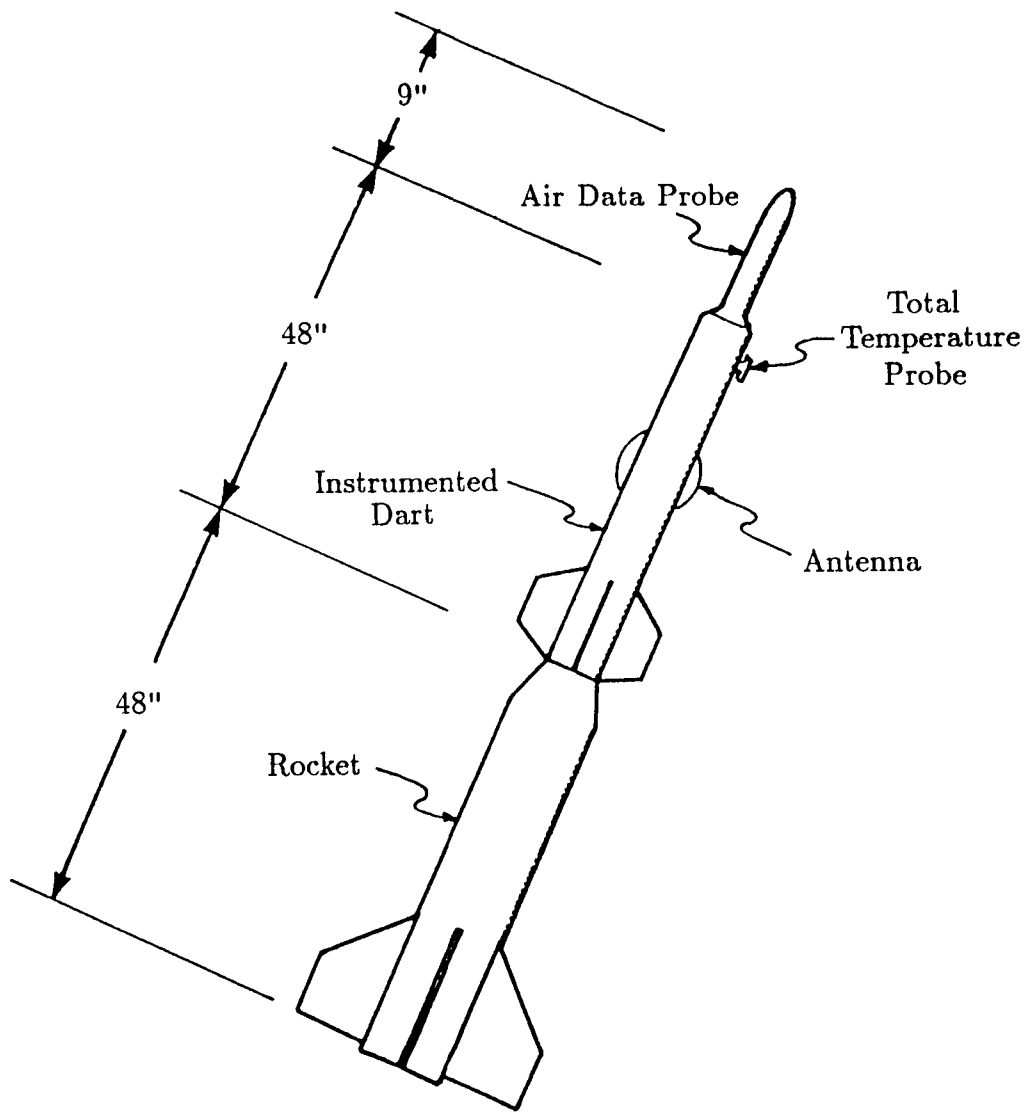


Figure 1.0 Rocket and Dart Concept.



of wind velocity in support of atmospheric research, the F-104 and ER-2 airplanes have been used to determine wind velocity profiles for potential shuttle launch support. Additionally, the trajectory and dynamics unique to a rocket will be considered to simplify or improve the measurements required for the final wind calculations. The wind velocity calculation uncertainty will be quantified analytically using the Taylor's error propagation formula, based on the performance of meteorological rockets and commercially available instrumentation.

Note that NASA does not explicitly specify a minimum uncertainty to which winds aloft must be known. Potential loading on the ascending shuttle has been and continues to be evaluated from winds predicted from Jimsphere trajectories. Thus new methods of wind measurement must, at some point, be judged against the Jimsphere. Actual calculated winds from data gathered from an ascending rocket are not available for comparison against Jimsphere-derived winds. Therefore, for this study, the similarities between the system proposed for the rocket and the systems in place on airplanes dictate comparison of the data potentially gathered from the rocket to data gathered from airplanes.

## Chapter II

### Wind Vector Calculations from an Airborne Platform

Wind speed and direction, based on measurements made from an airborne platform, are calculated from the vector addition

$$\vec{W} = \vec{W}_{VC} + \vec{V}_{GS} \quad (2.1)$$

where  $\vec{W}$  is the wind velocity with respect to an observer on earth,  $\vec{W}_{VC}$  is the air velocity according to an observer on the airborne platform, and  $\vec{V}_{GS}$  is the platform velocity in the frame of the earth. In this report, contrary to the convention used by some meteorologists, the wind vector is positive in the direction of air flow. Measurements from the platform provide the information for air speed and direction in a coordinate system that rolls, pitches, and yaws with the platform. An inertial measurement system on board the vehicle measures the angles, angular velocity, and linear velocity which describe the platform motion and orientation with respect to the earth. With the air vector known in the moving coordinate system and the orientation of the moving coordinate system with respect to the earth known, the wind vector in the earthbound coordinate system can be calculated. Wind calculations based on measurements made from a rocket are identical in philosophy to those made from an airplane, although imaginary geometric reference planes must be established through the rocket for angle measurement references.

Wind velocity calculated from Equation (2.1) is extremely sensitive to the accuracy of the measurements used to calculate the velocity of air relative to the moving platform and the velocity of the moving platform relative to the earth. Both of these vectors have roughly the same magnitude, typically from mid-subsonic

Mach numbers to low supersonic Mach numbers, with nearly opposite directions. The difference in these large vectors, which are nearly equal, is the wind velocity being sought. Small errors in the calculation of either variable in Equation (2.1), which may not be significant for other purposes, may cause large uncertainties in the calculated wind velocity.

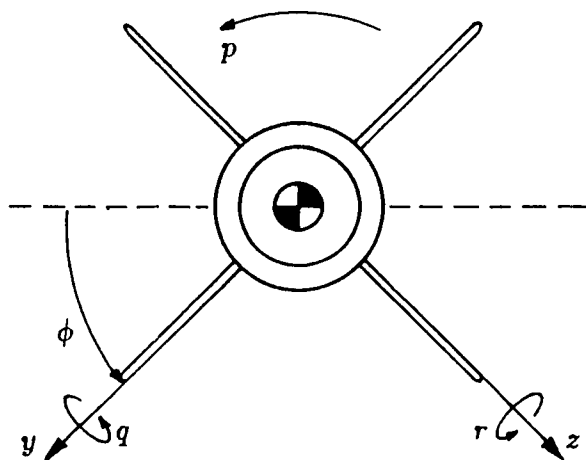
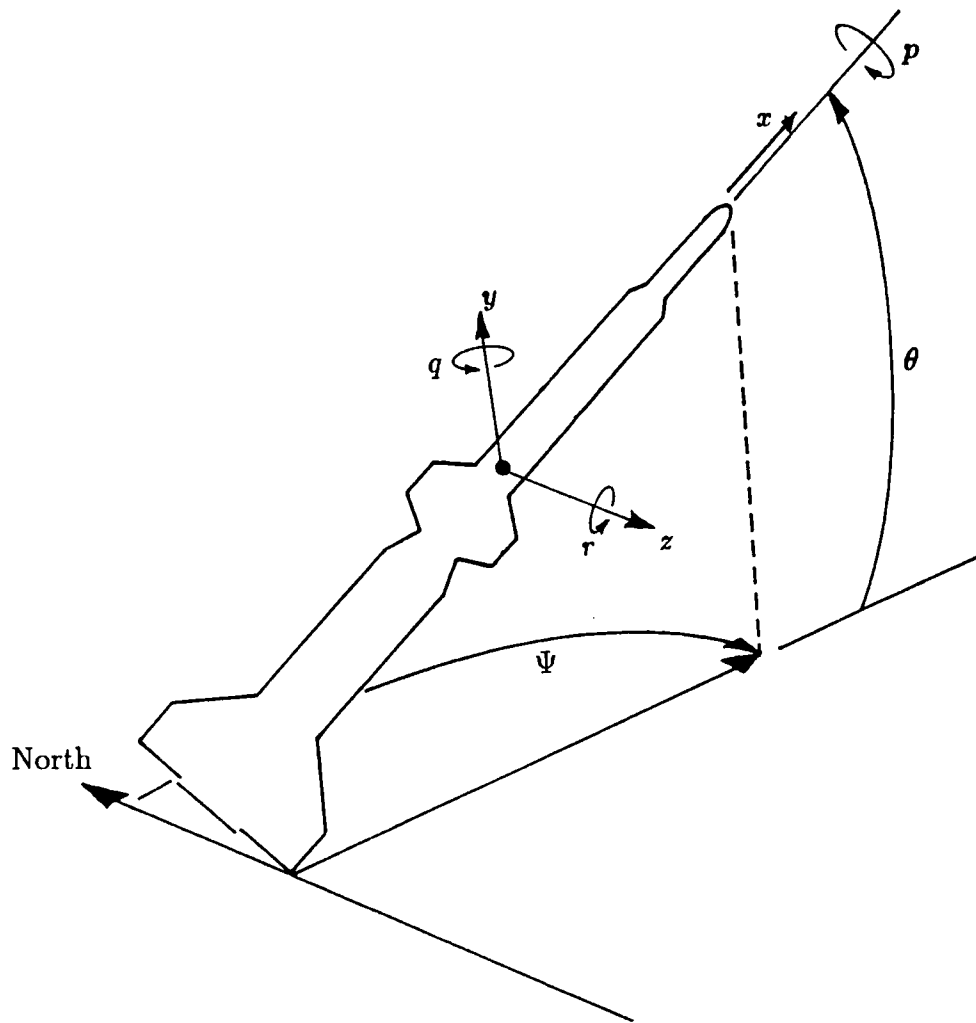
### Air Velocity

Air speed in the coordinate system fixed to an airplane (the true airspeed of the airplane), is calculated from total pressure, ambient pressure, and total temperature measurements. Etkin [6] calls this coordinate system the body-fixed coordinates, which is defined as having the x-axis pointing forward through the airplane nose along the airplane centerline, the y-axis pointing out the starboard wing, and the z-axis pointing out the bottom of the fuselage. The origin of the coordinate system is located at the airplane center of gravity. With imaginary horizontal and vertical planes defined, the body-fixed coordinate system can be related to a rocket, as shown in Figure 2.1.

The speed of compressible fluid flow can be shown to be determined by the flow Mach number and total temperature by

$$V_a = \frac{\sqrt{\gamma R T_o} M}{1 + \frac{\gamma+1}{2} M^2} \quad (2.2)$$

where  $V_a$  is the air speed,  $\gamma$  is the ratio of specific heats for air,  $R$  is the ideal gas constant for air,  $T_o$  is the total temperature of the air, and  $M$  is the Mach number. In this report,  $\gamma$  is treated as a constant, 1.4, because of the altitudes of interest for wind calculations. The Mach number when the rocket is traveling subsonically is calculated from the total and static pressures according to the expression



$x, y, z$  - Body-fixed axes  
 $p, q, r$  - Body-fixed rotation rates  
 $\phi, \theta, \Psi$  - Euler angles

**Figure 2.1 Body-fixed and Vehicle-centered Coordinate Frames and Euler Angles.**

$$M = \sqrt{\left[ \left( \frac{p_t}{p_s} \right)^{\frac{\gamma-1}{\gamma}} - 1 \right] \left[ \frac{2}{\gamma-1} \right]} \quad (2.3)$$

where  $p_t$  is the total pressure, and  $p_s$  is the static pressure.

When the vehicle is traveling supersonically, a shock wave in front of the rocket will reduce the total pressure and increase the static pressure, compared to the total pressure and static pressure on the upstream side of the shock wave. Although the measured total pressure will be reduced from the free stream conditions by the shock wave, the measured static pressure will be a fraction of the ambient pressure, dependent on the location of the static pressure measurement. For the airspeed calculation, the free stream Mach number (on the supersonic side of the shock wave) is calculated from the measured total pressure and free stream static pressure by solution of the Rayleigh supersonic pitot tube formula (Shapiro [7])

$$\frac{p_{t2}}{p_{s1}} = \frac{\left( \frac{\gamma+1}{2} M_1^2 \right)^{\frac{\gamma}{\gamma-1}}}{\left( \frac{2\gamma}{\gamma+1} M_1^2 - \frac{\gamma-1}{\gamma+1} \right)^{\frac{1}{\gamma-1}}} \quad (2.4)$$

where  $p_{t2}$  is the total pressure of the air flow, measured behind a normal shock wave,  $p_{s1}$  is the free stream static pressure, and  $M_1$  is the free stream Mach number.

The direction of the air relative to the probe is described by the angle-of-attack,  $\alpha$ , and sideslip angle,  $\beta$ , shown in Figure 2.2. In the body-fixed coordinate system, the air vector is defined by Lenschow [10] as

$$\vec{W}_{BF} = -V_a \begin{pmatrix} D^{-1} \\ D^{-1} \tan \beta \\ D^{-1} \tan \alpha \end{pmatrix} \quad (2.5)$$

where  $D = (1 + \tan^2 \alpha + \tan^2 \beta)^{1/2}$ . Equation (2.9) can be derived by the decomposition of the air velocity as shown in Figure 2.3.

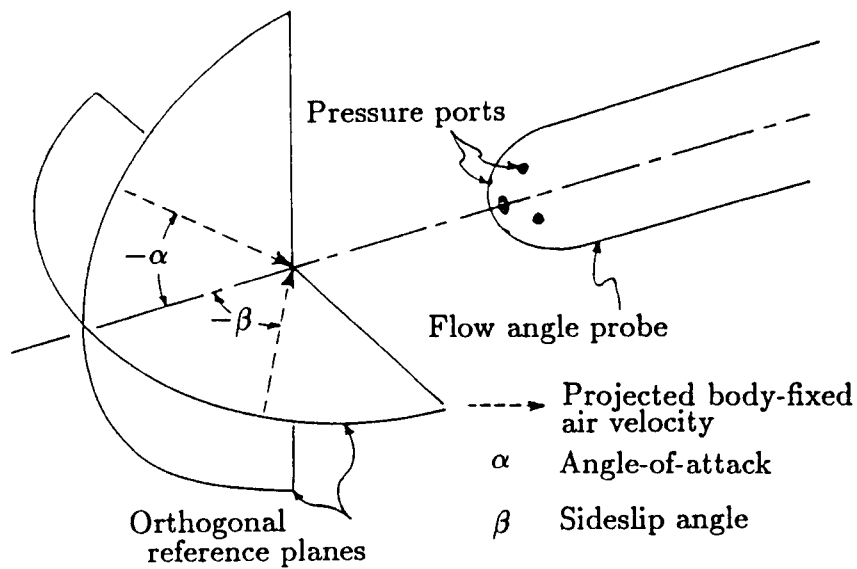


Figure 2.2 Angle-of-attack and Sideslip Angle Definitions [16].

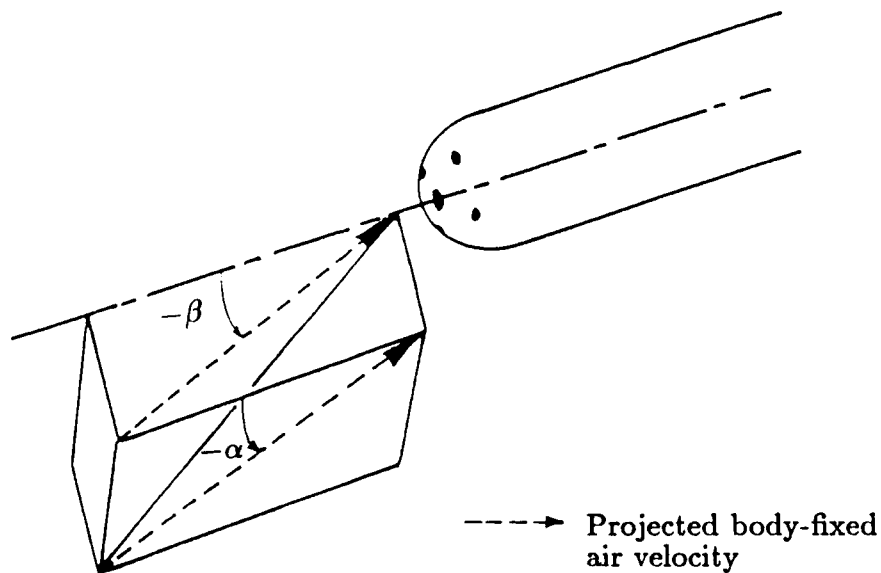


Figure 2.3 Air Velocity Decomposition

As the vehicle rolls, pitches, and yaws, the velocity of the probe used for the air speed measurements induces an air velocity equal to

$$\begin{pmatrix} p \\ q \\ r \end{pmatrix} \times \begin{pmatrix} l_x \\ l_y \\ l_z \end{pmatrix} \quad (2.6)$$

where the vector  $(p, q, r)$  is the rotation rate of the vehicle in the body-fixed frame, an  $(l_x, l_y, l_z)$  is the position of the probe in the body-fixed frame. For airplane based measurements, this quantity is considered negligible unless the airplane is maneuvering. Likewise for rocket based measurements, the induced velocity of (2.6) will be negligible. Only  $p$ , the long axis spin of the rocket, will be consequential, and, by design, the probe will be located on the long axis. Thus (2.6) will be small compared to the final wind velocity. Therefore the air velocity induced by the rotation rate of the rocket will be ignored herein.

### Rotation Transformation

The vehicle-centered vertical frame, as defined by Etkin [6], has its origin fixed at the airplane center of gravity, with the x-axis pointed north, the y-axis pointed east, and the z-axis pointed in the direction of the local gravity vector. Etkin [6] derives the transformation of a vector from body-fixed to vehicle-centered vertical coordinates as

$$\vec{W}_{VC} = \mathbf{L}_{\mathbf{BV}}^{-1} \vec{W}_{BF} \quad (2.7)$$

with

$$\mathbf{L}_{\mathbf{BV}} = \begin{pmatrix} \cos \theta & \sin \phi \sin \theta \cos \psi & \cos \phi \sin \theta \cos \psi \\ \cos \theta \sin \psi & -\cos \phi \sin \psi & +\sin \phi \sin \psi \\ -\sin \theta & \sin \phi \sin \theta \sin \psi & \cos \phi \sin \theta \sin \psi \\ & +\cos \phi \cos \psi & -\sin \phi \cos \psi \\ & \sin \phi \cos \theta & \cos \phi \cos \theta \end{pmatrix} \quad (2.8)$$

where  $\phi$  is the airplane bank angle,  $\theta$  is the airplane elevation angle, and  $\psi$  is the airplane heading. The angles  $\phi$ ,  $\theta$ , and  $\psi$ , called the Euler angles, are shown in Figure 2.1.

### Velocity Transformation

The vehicle-centered vertical frame and the earth-surface frame differ only in the relative velocity between their respective origins. Thus the transformation of a vector from the former to the latter involves only the addition of the velocity of the vehicle-centered vertical frame relative to earth-surface. This relative velocity is simply the ground speed of the vehicle:

$$\vec{W} = \vec{W}_{VC} + \vec{V}_{GS} \quad (2.1)$$

### Summary

The velocity of the air relative to the earth is calculated by transforming the air velocity relative to the rocket by coordinate rotation and coordinate translation to the frame of the earth. Furthermore, the measured magnitude of the air speed must be transformed across a normal shock wave for supersonic rocket flight. The three vectors of secondary interest are then the air velocity (air speed, angle of attack, and sideslip angle), rocket attitude (bank, elevation, and heading), and rocket velocity (north, east, and vertical speeds). These operations are done by



$$\vec{W} = \vec{V}_{GS} - V_a \mathbf{L}_{\mathbf{BV}}^{-1} \begin{pmatrix} D^{-1} \\ D^{-1} \tan \beta \\ D^{-1} \tan \alpha \end{pmatrix} \quad (2.9)$$

where  $V_a$  is found by Equation (2.2) and (2.3) in subsonic flight, and (2.2) and (2.4) in supersonic flight.

## Chapter III

### Measurements and Instrumentation

The instrumentation on the rocket necessary for wind velocity calculations provides the information needed to determine the air velocity relative to the rocket, the orientation in three dimensions of the rocket relative to the Earth, and the linear velocity of the rocket relative to the Earth. The air speed relative to the rocket is calculated with total and static pressure measurements, two differential pressure measurements, and one temperature measurement. The direction of the air relative to the rocket, described by the angle of attack and sideslip angle,  $\alpha$  and  $\beta$ , would be determined from a calibrated probe with two differential pressure measurements. The orientation of the rocket, described by the bank, elevation, and heading of the rocket, would be determined by gyroscopes, angular rate measurements, or a combination of the two. The earth-surface velocity of the rocket, the rocket ground speed, would be determined by three orthogonal acceleration measurements. Thus, the instrumentation will provide for:

- 1) total and static pressure measurements,
- 2) two flow angle measurements,
- 3) one temperature measurement,
- 4) three angular or angular rate measurements, and
- 5) three linear acceleration measurements.

The instruments listed are representative of the instruments used on airplanes for wind velocity calculations. However, this pallet may be simplified without data compromise due to the nature of the rocket flight and motions.

## Airspeed

The vehicle airspeed is calculated from compressible flow theory and three measurements to be made from the rocket: stagnation pressure, static pressure, and stagnation temperature of the air stream in the frame of the moving rocket.

Chue [11] and Gracey [12] state that total pressure is measured accurately with both blunt and streamlined pitot tubes, although Chue [11] reports corrections are necessary for viscous effects in flows with Reynold's numbers less than 1000. Gracey [12] also states that total pressure measurements are independent of small incidence angles, for appropriately shaped probes.

The accuracy of the static pressure measurement is highly dependent on the location of the pressure ports, either on the pitot probe or possibly on the dart. Chue [11] and Gracey [12] show corrections necessary for static pressure measurements with probes for flow Mach number, Reynold's number, incidence angle, and port location. Data in Figure 3.1 [8] suggest that for the hemispherical probe considered herein, the measured static pressure would be 95 to 100% of the true ambient pressure, except near unity Mach number. However, because of the unique geometry of the probe, dart, and motor combination, wind tunnel calibration would be necessary for the range of anticipated Mach number and flow incidence range to correlate the measured pressure to the true pressure. An easier method might be to correlate the ratio of the measured static pressure and the total measure to the true Mach number, similarly to the method in Vahl [13].

Because of the transient nature of the pressures to be measured from the rocket and the volume of the tubes necessary between the pressure transducers and the pressure ports, a lag would exist between the true pressures and the measured pressures. The pressure lags could be modeled, and the measurements possibly compensated digitally, as done, for example, by Brown [14]. The effect

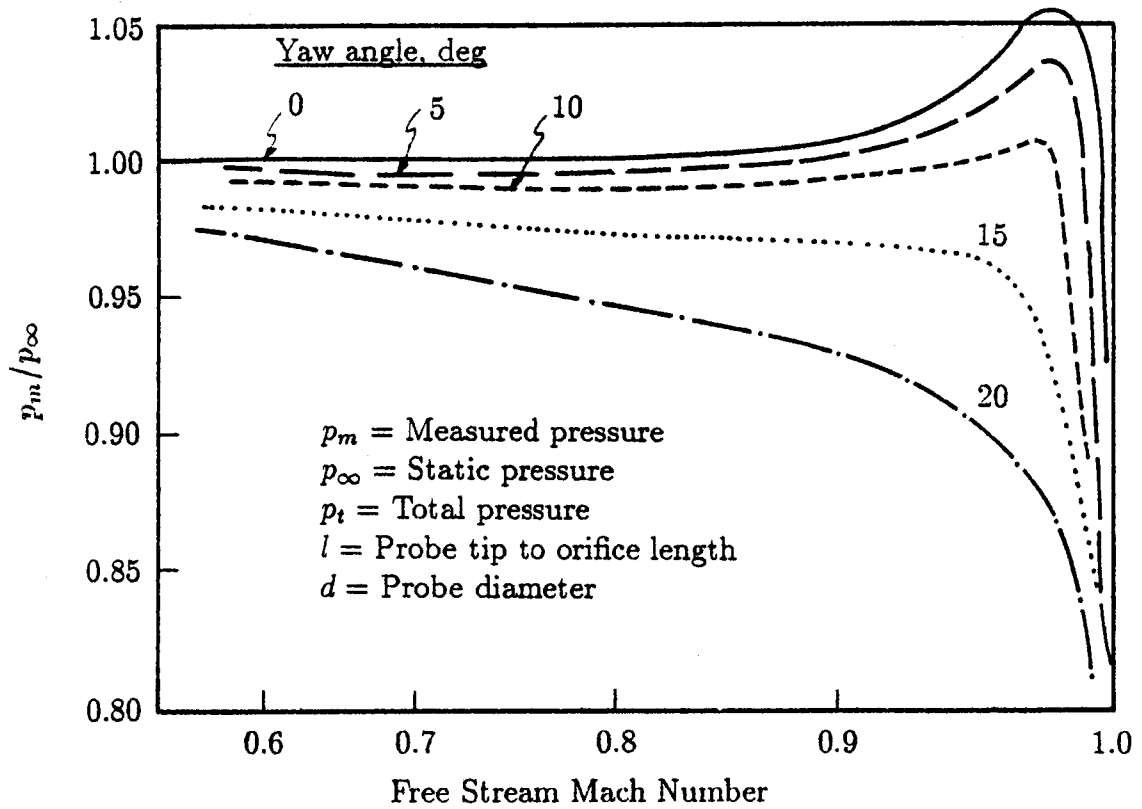


**Figure 3.1** Effects of Mach Number and Yaw on the Reading of a Static Tube at  $l/d = 3$  (Adapted from Howarth, et al. [8]).

of the tubing is, to some extent, desirable, for filtering the high frequencies in the data due to atmospheric eddies.

The total temperature potentially would be measured outside the rocket boundary layer, by a total temperature probe using a thermocouple, thermistor, or resistance temperature device (RTD). Both the F-104 and the ER-2 airplanes have total temperature measurements from a transducer mounted on the end of a strut mounted on their respective fuselages. Similarly, the rocket would have a strut mounted temperature transducer on the body of the payload portion of the rocket or on an air data probe extending from the rocket. Similarly to the static pressure measurement, the measured total temperature would be correlated to the true total temperature by the Mach number dependent recovery factor. Figure 3.2 [9] shows an airspeed dependent recovery factor for a Pratt and Whitney total temperature probe, which is typical for any total temperature probe.

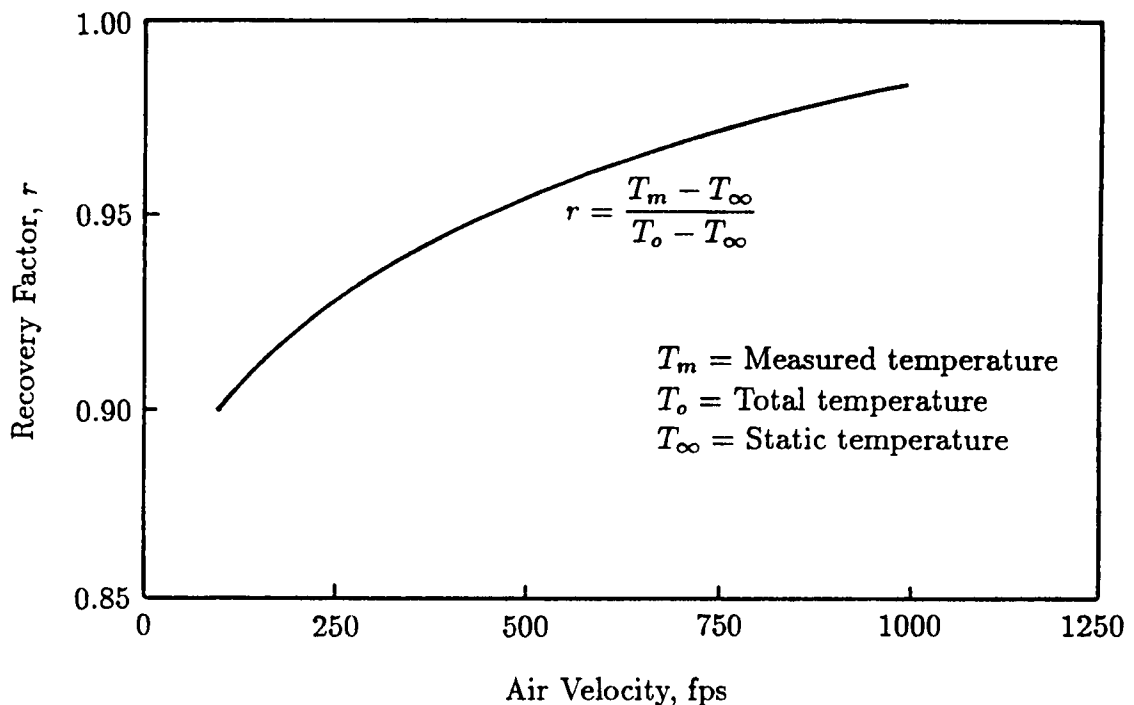


**Figure 3.2 Recovery Factor for a Pratt and Whitney Total Temperature Probe (Adapted from Volluz [9]).**

In this thesis, the total pressure measurement, the static pressure measurement, and the total temperature measurement will be assumed to be related to true conditions from wind tunnel calibrations to within the accuracy of the transducers making the measurements. Because the incidence angles are anticipated to be small (discussed in Chapter VI) and the range of Reynold's numbers will be high ( $10^6 \text{ ft}^{-1}$ ), the necessary corrections are anticipated to be only Mach number dependent.

### Flow Angle

The angle of airflow relative to the rocket is measured in two reference planes, corresponding to angle-of-attack and sideslip angle for airplanes. The Dryden F-104 and the Ames ER-2 airplanes use different methods for measuring these angles, either of which is potentially useful for a rocket application. The Dryden F-104 airplane uses flow vanes, as shown in Figure 3.3, and the Ames ER-2 airplane uses differential pressure measurements on the radome (Figure 3.4) which are correlated to particular flow angles.

The standard NACA air data probe, which is used by the Dryden F-104 airplane, is equipped with vanes which measure airflow by vane displacement. The actual flow angle is found by correcting the displacement angle according to wind tunnel calibrations for varying Mach number, angle-of-attack and sideslip.

Similarly to the differential pressure measurement system on the ER-2 airplane, probes are made to measure flow angles and flight Mach number for airplanes and wind tunnels from differential pressure measurements. Examples of a Conrad probe, a conical probe, and a hemispherical probe are shown in Figure 3.5. The flow angle in a plane corresponding to the plane of a differential pressure measurement is calculated from Scott, et al. [15] and Rosemount [16] by

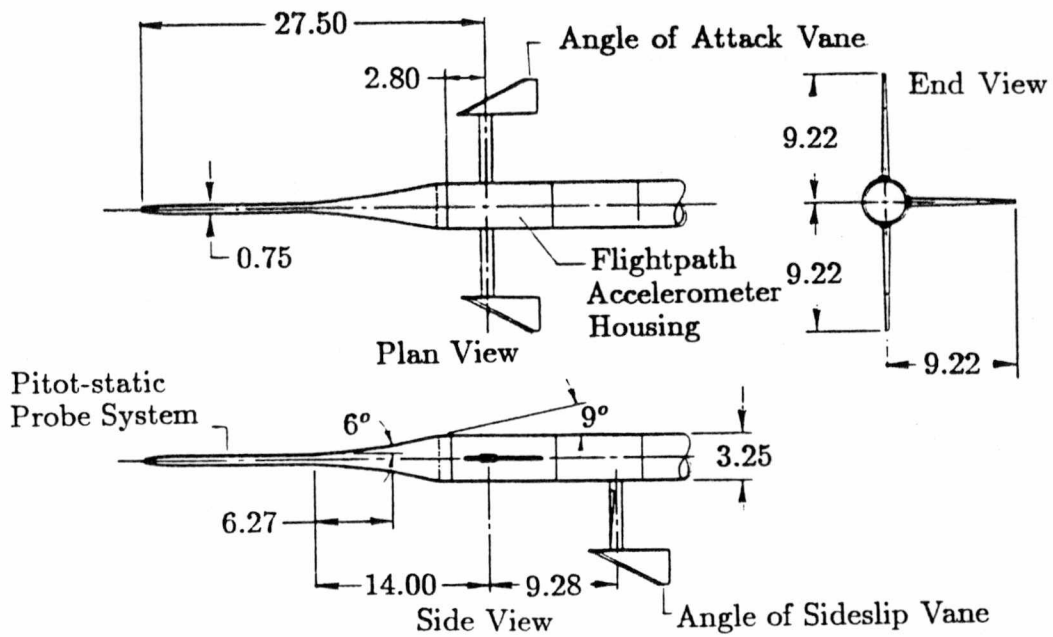


Figure 3.3 Free Vanes on an Air Data Probe for Angle Measurements [31].

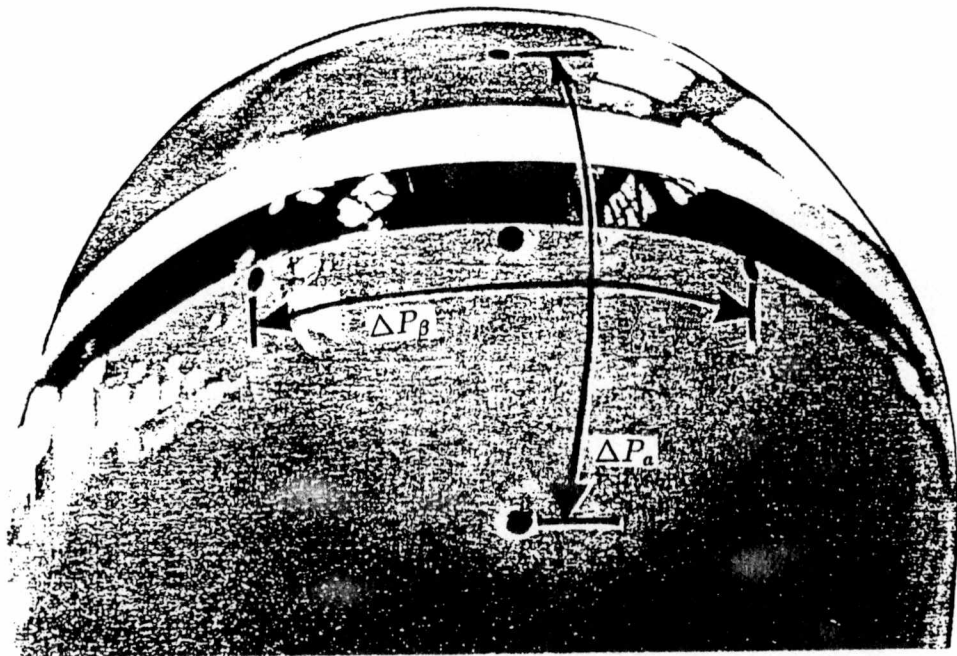


Figure 3.4 ER-2 Radome with Angle-of-Attack and Sideslip Angle Pressure Ports [15].

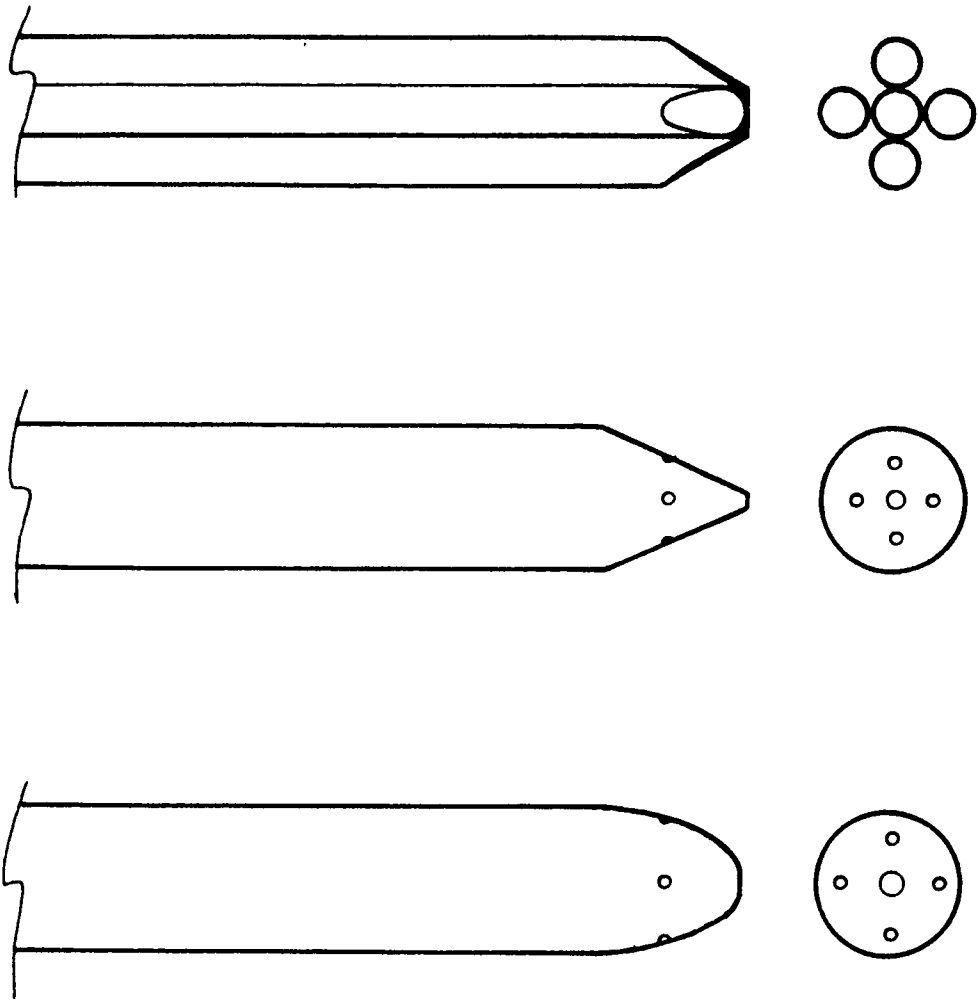


Figure 3.5 Conrad, Conical, and Hemispherical Flow Angle Probes.



$$\alpha = \frac{\Delta p}{kq} \quad (3.1)$$

where  $\alpha$  is the flow angle,  $\Delta p$  is the differential pressure,  $k$  is the air flow angle sensitivity factor, and  $q$  is the dynamic pressure,  $p_t - p_s$ . The airflow angle sensitivity factor would be found from wind tunnel calibrations and is roughly constant within small Mach number domains. Vahl, et al. [13] report an iterative method of calculating flow Mach number and angles, using a conical probe without a static pressure measurement, whereby the ratio of the mean pressure measured at the inclined ports to the total pressure is correlated to the free stream Mach number. The flow angles are correlated to the ideal gas dynamic pressure of the indicated Mach number through Equation (3.1), where  $k$  is a function of the Mach number. The indicated Mach number is corrected for the flow angle on the probe, and the flow angles are recalculated. The process continues until the Mach number converges.

Dudzinski and Krause [17] report that in flows with Mach numbers ranging from 0.3 to 0.9, the worst case flow angle uncertainty (in low velocity or low density flows) determined from measurements with a Conrad probe was less than  $0.5^\circ$  and “several times smaller” with high velocity or high density conditions. Furthermore, these uncertainties were attributed to the resolution of the differential pressure measurement (0.5 mm H<sub>2</sub>O).

Gaillard [18] reports measured flow angles with an accuracy of 0.2 deg with a 60 deg conical probe for flows with Mach numbers ranging from 0.6 to 2.6 and a flow angles of less than 20 deg. For flow angles greater than 20 deg, the measurement accuracy degenerates to 0.4 deg.

Bryer and Pankhurst [19] recommend a hemispherical probe for high subsonic,

transonic, and low supersonic flow, rather than a sharp ended probe, because the shock wave resulting from the presence of the probe is always detached from the blunt probe. Rosemount claims a flow angle accuracy of 0.2 deg, without correction for manufacturing anomalies, for a hemispherical probe. Hagen [20] claims an accuracy of 0.1 deg is possible with that probe with corrections for the pressure port misalignments.

Note that the previously mentioned accuracies for flow angle measurements with small differential pressure probes have been obtained in wind tunnels. However, Brown [21] and Poellet [22] report accuracies of 0.13 deg and 0.1 deg, respectively, for flow angle measurements with the Rosemount probe on airplanes flying subsonically.

A possible method of determining the angles of attack and sideslip would be to measure the angular acceleration of the dart due to sideloading from the wind. The angular acceleration of the rocket would be proportional to the sideloading and inversely proportional to the moment of inertia of the rocket. The angular acceleration of the rocket could thus be correlated to the angles of attack and sideslip. However, determination of the moment of inertia would be difficult because of the changing mass of the rocket motor (from burning propellant) and the spin of the rocket.

### Rocket Inertial Motion

Inertial Navigation Systems provide the vehicle attitude (bank, elevation, and heading) and ground velocity for the wind velocity calculations of both the ER-2 and the F-104 airplanes. Radar tracking was also used for more accurate ground velocity calculations for the F-104 airplane. The cost and size restraints of an expendable rocket borne platform preclude the use of an INS; however, the

components of an INS used to make the inertial measurements (gyroscopes and accelerometers) could be used on the rocket.

INS's use gyroscopes to measure the angular displacement of the INS from a reference plane. Gyroscopic output signals are correlated to either the net angular displacement of the gyroscope from an reference or the discrete angular displacement from a previous time step. In the case of a spinning rocket, the former could not be used to measure the bank angle; these types of gyroscopes are limited typically to a net displacement of less than 90 deg, whereas spin rates for meteo-logical rockets are typically several revolutions per second. The spin rate can be calculated by accelerometer measurements by virtue of gravity; an accelerometer suite (which will be discussed in the context of the ground velocity calculation) would have accelerometers on the two non-spinning axes of the rocket (the y and z-axes in the body-fixed coordinates). These accelerometers would periodically measure a component of gravity with a frequency equal to the spin rate of the rocket, assuming the rocket ascended with an elevation angle representative of the elevation angle of the ascending space shuttle (60 deg) at the same altitudes. Thus, the phase of the accelerometer measurements would be correlated to the bank angle. Furthermore, the magnitude of the sinusoidal component of the accelerometer measurements could be correlated to the elevation angle of the rocket. The sinusoidal component of the accelerometer measurements would be separated by a digital bandpass filtering based on the spin rate of the rocket.

Rate measurements on the two axes off the long centerline of the rocket, combined with the spin rate of the rocket determined by the accelerometer suite, would be used to calculate the attitude of the rotating rocket by discrete rotations of the body-fixed axes. Instead of determining the Euler angles and then calculating the transformation matrix,  $L_{BV}$ , the transformation matrix would be

recalculated from the previous transformation matrix and the measured rotation rate of the rocket.

The rows of the transformation matrix are unit vectors in the directions of the body-fixed axis relative to the vehicle-centered axes. The rows of a new transformation matrix can be constructed after a discrete rotation of the body-fixed frame by

$$\vec{x}'_i = (\vec{x}_i \cdot \vec{\omega}) \frac{\vec{\omega}}{\omega^2} + \vec{R}'_i \quad (3.2)$$

where  $\vec{x}'_i$  is the unit vector on the  $i^{\text{th}}$  axis of the new body-fixed frame relative to the vehicle-centered frame,  $\vec{x}_i$  is the unit vector on the  $i^{\text{th}}$  axis of the old body-fixed frame,  $\vec{\omega}$  is the rotation rate vector in the old body fixed frame transformed to the vehicle-centered frame,  $\omega^2$  is the square of the magnitude of the rotation rate vector. The vector  $\vec{R}'_i$  is found from solution of the system

$$\vec{\omega} \cdot \vec{R}'_i = 0 \quad (3.3)$$

$$\vec{R}_i \cdot \vec{R}'_i = R^2 \cos \theta \quad (3.4)$$

$$(\vec{\omega} \times \vec{R}_i) \cdot \vec{R}'_i = \omega R^2 \sin \theta \quad (3.5)$$

where  $\theta$  is the discrete three dimensional rotation magnitude, and  $\vec{R}'_i$  is equal to  $\vec{x}'_i - (\vec{x}'_i \cdot \vec{\omega})\vec{\omega}/\omega^2$ . The initial attitude of the rocket would be the initial condition required for the solution of this discrete, single integration. The derivation of this solution by the author is given in the Appendix, although this derivation can probably be found elsewhere in the context of strap-down INS operations principles.

The ground velocity of the rocket would be determined by the transformation and integration of three orthogonal acceleration measurements in the body-fixed

frame. An accelerometer suite would be fixed to the dart body and would rotate with the rocket. The time dependent inertial velocity of the rocket would be determined by

$$\vec{V}_{GS} = \int_{t_o}^t \mathbf{L}_{\mathbf{BV}}^{-1} \vec{a}_{BF} d\tau \quad (3.6)$$

where  $\vec{V}_{GS}$  is the inertial velocity,  $t$  is time,  $t_o$  is the time of launch,  $\mathbf{L}_{\mathbf{BV}}^{-1}$  is the transformation matrix from Equation (2.8), and  $\vec{a}_{BF}$  is the measured acceleration of the rocket in the body-fixed frame.

### Data Sampling

The anticipated dynamics of the rocket and dart, combined with the necessity of simultaneous measurements of the more rapidly changing parameters measured from the rocket (such as flow angle and bank angle), require that some attention be given to the instrumentation sampling scheme. Typically, measurements are compensated for the time delay necessary between the sequential interrogation of instrumentation, such as is done with the data collected on the ER-2 airplane. However, electronics are readily available with which several data channels can be effectively interrogated simultaneously, negating the necessity for time compensation. Such an approach would probably be used on the rocket.

## Chapter IV

### Uncertainty Analysis

Three equations are developed herein, which can be combined to make one equation, which show the approximate relationship between the uncertainties in the measurements made from the rocket and the uncertainty in the calculated wind velocity. The uncertainty of the calculated wind velocity is shown to Mach number dependent.

The uncertainty in the calculation of a wind vector from measurements made on an airborne platform will be developed with the Taylor's series method of error propagation

$$(\Delta F)^2 = \sum_{i=1}^n \left( \frac{\partial F}{\partial \xi_i} \right)^2 (\Delta \xi_i)^2 \quad (4.1)$$

where  $F$  is the calculated parameter of interest and the set of  $\xi_i$  are the independent variables, or measurements, governing  $F$ . The assumption is made by use of (4.1) that the uncertainties in  $\xi_i$  are uncorrelated.

In the case of wind calculations supported from an airborne measurements, Equations (2.1), (2.7), (2.8), and (3.6) can be substituted into (4.1) and the uncertainty in the calculated wind velocity can be shown to be

$$\left( \frac{\Delta W}{V_a} \right)^2 = \frac{t^2 (\Delta a)^2}{V_a^2} + \left( \frac{\Delta W_{BF}}{V_a} \right)^2 + 4(\Delta \phi)^2 \quad (4.2)$$

where  $\Delta W$  is the root mean square of the earth-surface wind component uncertainties,  $t$  is the time from rocket launch,  $\Delta a$  is the platform acceleration measurement uncertainty,  $\Delta W_{BF}$  is the root mean square of the body-fixed air velocity component uncertainties, and  $\Delta \phi$  is the uncertainty of the measured or calculated Euler

angles. Figure 4.1 shows, from Equation (4.2), the uncertainty in the earth-surface wind velocity from the body-fixed wind velocity uncertainty, the uncertainty in the Euler angles  $\phi$ ,  $\theta$ , and  $\psi$ , and the airspeed. The assumptions are made in Equation (4.2) that the Euler angle uncertainties are all of equal magnitude and that the uncertainties in the three measured acceleration components are all of equal magnitude.

At this point, the rotation rate of the vehicle should be considered in the error analysis. As the vehicle rotates, a wind vector is induced at the wind speed instrumentation proportional to the rotation rate and the distance between the airplane center of gravity (c.o.g.) and the wind speed instrumentation. However, the product of the rotation rate and length between the c.o.g. and instrumentation is small for a meteorological rocket and the contribution to the measured wind speed is not significant. Thus, the error contributed by the measured rate of the vehicle rotation will be neglected here.

The three components of the wind vector in the body-fixed frame,  $W_x$ ,  $W_y$ , and  $W_z$ , are calculated from the airspeed of the vehicle,  $V_a$ , the angle of attack,  $\alpha$ , and sideslip angle,  $\beta$ , between the vehicle and relative wind, by Equation (2.5). Equation (2.5) can be substituted into (4.1), simplified by small angle assumptions, and normalized by the airspeed to

$$\left(\frac{\Delta W_{BF}}{V_a}\right)^2 = \left(\frac{\Delta V_a}{V_a}\right)^2 + 2(\Delta\alpha)^2 \quad (4.3)$$

where  $\Delta V_a$  is the uncertainty in the calculated airspeed, and  $\Delta\alpha$  is the uncertainty of the calculated flow angles. This relation is shown in Figure 4.2.

The uncertainty of the calculated airspeed can be shown to be a function of the

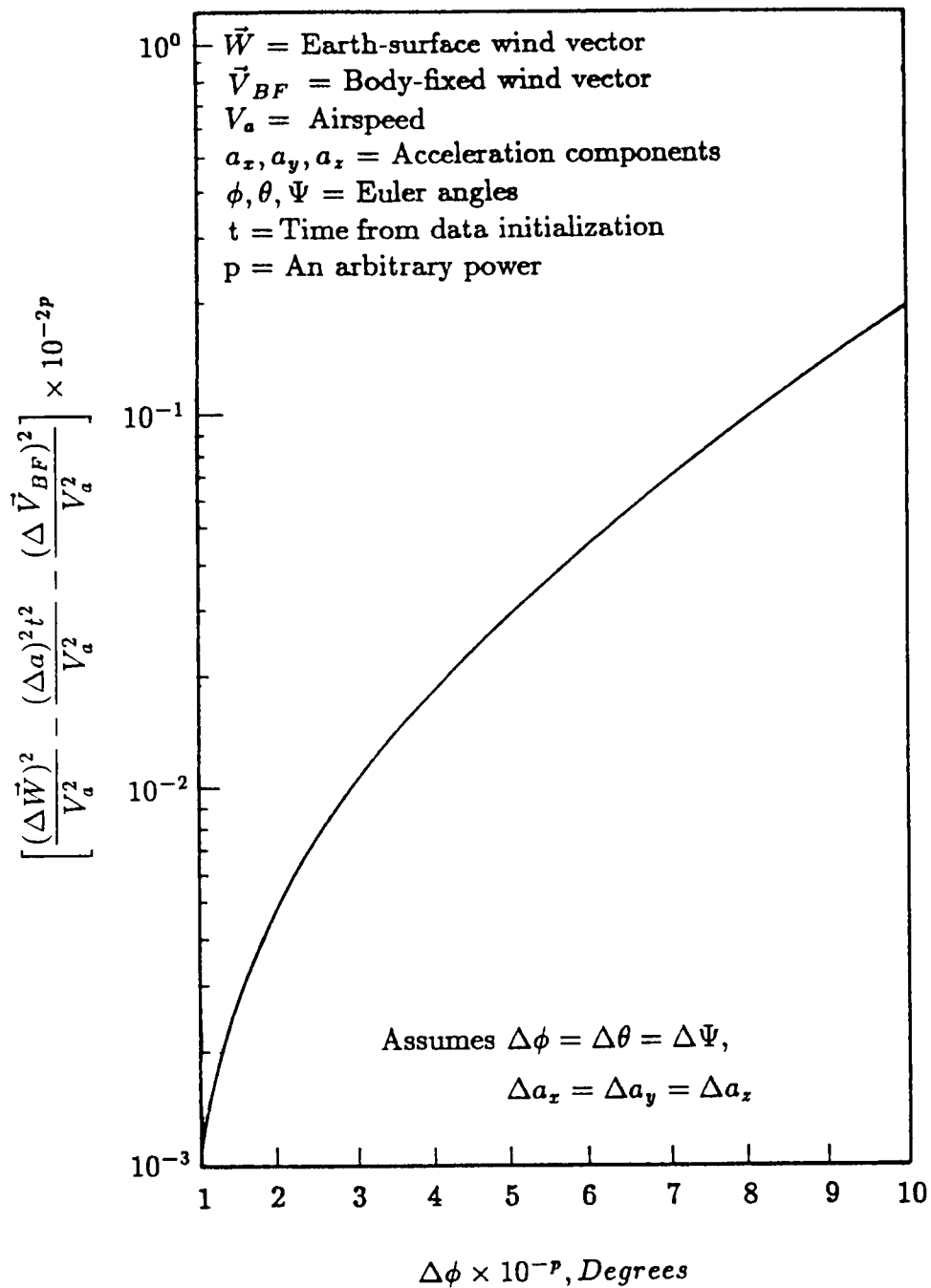


Figure 4.1 Wind Vector Uncertainty from Body-fixed Wind Vector Uncertainty, Acceleration Measurement Uncertainty, Euler Angle Uncertainty, and Airspeed.



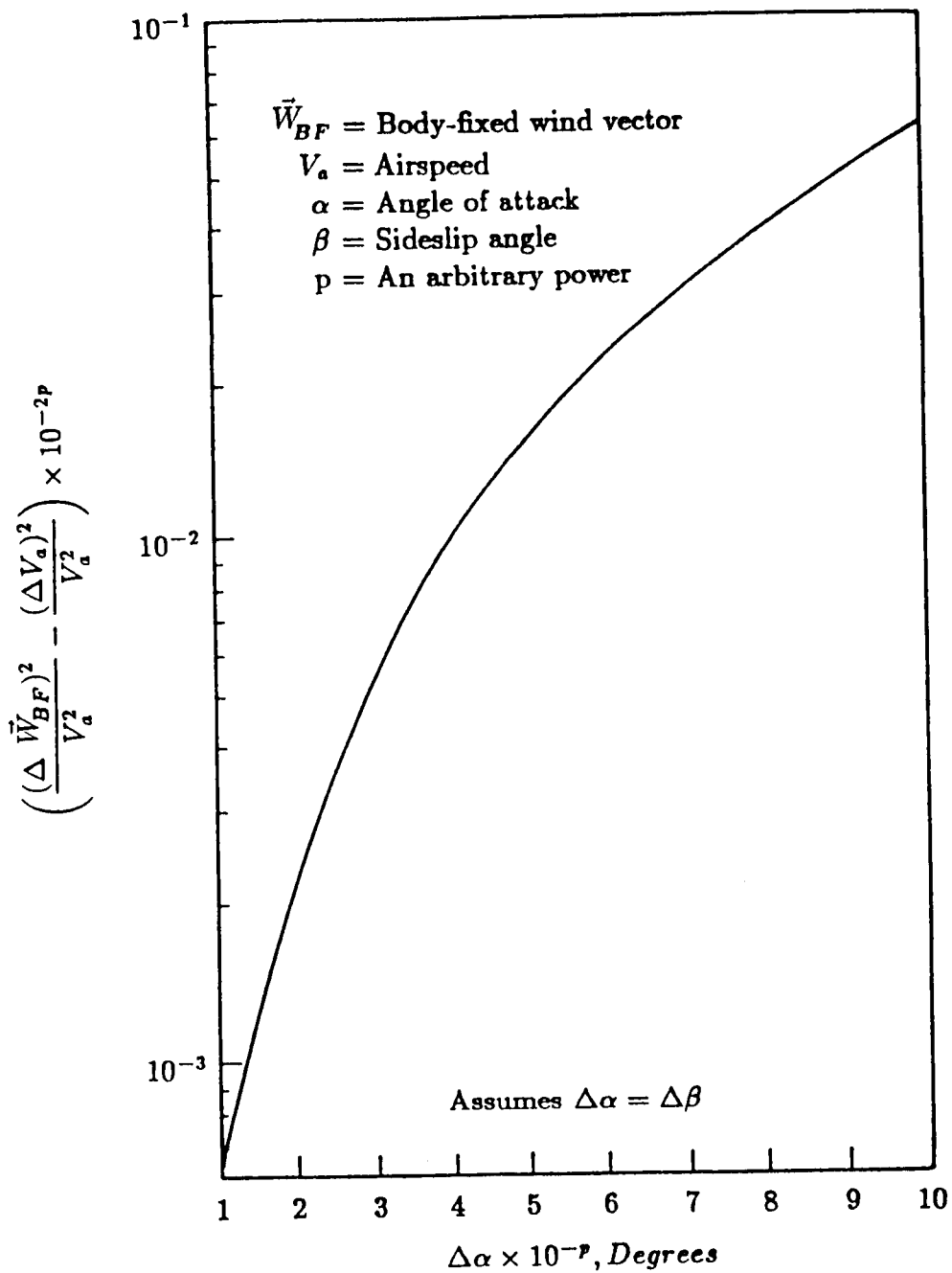


Figure 4.2 Body-fixed Wind Velocity Uncertainty from Airspeed and Flow Angle Uncertainties.

total temperature measurement uncertainty and the uncertainty of the calculated Mach number by

$$\left(\frac{\Delta V_a}{V_a}\right)^2 = \frac{1}{4}\left(\frac{\Delta T_o}{T_o}\right)^2 + \frac{1}{4}\left(\frac{1}{1 + \frac{\gamma-1}{2}M^2}\right)^2 \left(\frac{\Delta M^2}{M^2}\right)^2 \quad (4.4)$$

The uncertainty in the subsonic Mach number is calculated from the uncertainty in the calculated pressure ratio by

$$(\Delta M^2)^2 = \left(\frac{2}{k}\left(1 + \frac{\gamma-1}{2}M^2\right)\right)^2 \left(\Delta \frac{p_t}{p_s}\right)^2 / \left(\frac{p_t}{p_s}\right)^2 \quad (4.5)$$

The uncertainty in the pressure ratio  $\frac{p_t}{p_s}$  is evaluated from the two remaining independent variables in the wind velocity calculation

$$\left(\Delta \frac{p_t}{p_s}\right)^2 / \left(\frac{p_t}{p_s}\right)^2 = \left(\frac{\Delta p_s}{p_s}\right)^2 + \left(\frac{\Delta p_t}{p_t}\right)^2 \quad (4.6)$$

For convenience, the relative total and static pressure measurement uncertainties will be considered equal, so

$$\left(\Delta \frac{p_t}{p_s}\right)^2 / \left(\frac{p_t}{p_s}\right)^2 = 2\left(\frac{\Delta p_s}{p_s}\right)^2 \quad (4.7)$$

Thus, the uncertainty in the calculated subsonic airspeed is approximated by

$$\left(\frac{\Delta V_a}{V_a}\right)^2 = \frac{1}{4}\left(\frac{\Delta T_o}{T_o}\right)^2 + \frac{2}{\gamma^2 M^4} \left(\frac{\Delta p_s}{p_s}\right)^2 \quad (4.8)$$

Note that the uncertainty of the free stream pressure measurement will probably be greater than the uncertainty in the total pressure measurement, because of the probe body effects on the free stream pressure (discussed in Chapter III).

The uncertainty in the supersonic Mach number can be shown from Equation (2.4) to be

$$\left(\frac{\Delta M^2}{M^2}\right)^2 = \left(\frac{M^2 - \frac{\gamma-1}{2\gamma}}{M^2 - \frac{1}{2}}\right)^2 \left(\Delta \frac{p_t}{p_s}\right)^2 / \left(\frac{p_t}{p_s}\right)^2 \quad (4.9)$$

and the resulting supersonic airspeed uncertainty can be shown to be

$$\left(\frac{\Delta V_a}{V_a}\right)^2 = \frac{1}{4} \left(\frac{\Delta T_o}{T_o}\right)^2 + \frac{1}{2} \left(\frac{1}{1 + \frac{\gamma-1}{2} M^2}\right)^2 \left(\frac{M^2 - \frac{\gamma-1}{2\gamma}}{M^2 - \frac{1}{2}}\right)^2 \left(\frac{\Delta p_s}{p_s}\right)^2 \quad (4.10)$$

Figure 4.3 shows the uncertainty of the calculated airspeed based on the uncertainties of the pressure and temperature measurements from Equation (4.8) and (4.10).

### Summary

The uncertainty in wind velocity calculations from measurements made from a rocket-propelled dart is determined by the measured parameters  $\vec{a}_{BF}$ ,  $\phi$ ,  $\theta$ ,  $\psi$ ,  $T_o$ ,  $p$ ,  $p_o$ ,  $\alpha$ , and  $\beta$ , and their measurement uncertainties, and can be approximated by the relations given in Figures 4.1, 4.2, and 4.3. This neglects any contribution to the wind velocity made by the rotation rate of the dart, which is small, and errors in the alignment of the instruments making the flow angle, attitude, and acceleration measurements. The alignment of these instruments will be assumed to be within 0.01 deg or correctable to within 0.01 deg, based on the alignment errors reported by Haering [23] of the instruments on the F-104 airplane, which is well within the instrument uncertainties (discussed in Chapter VI).

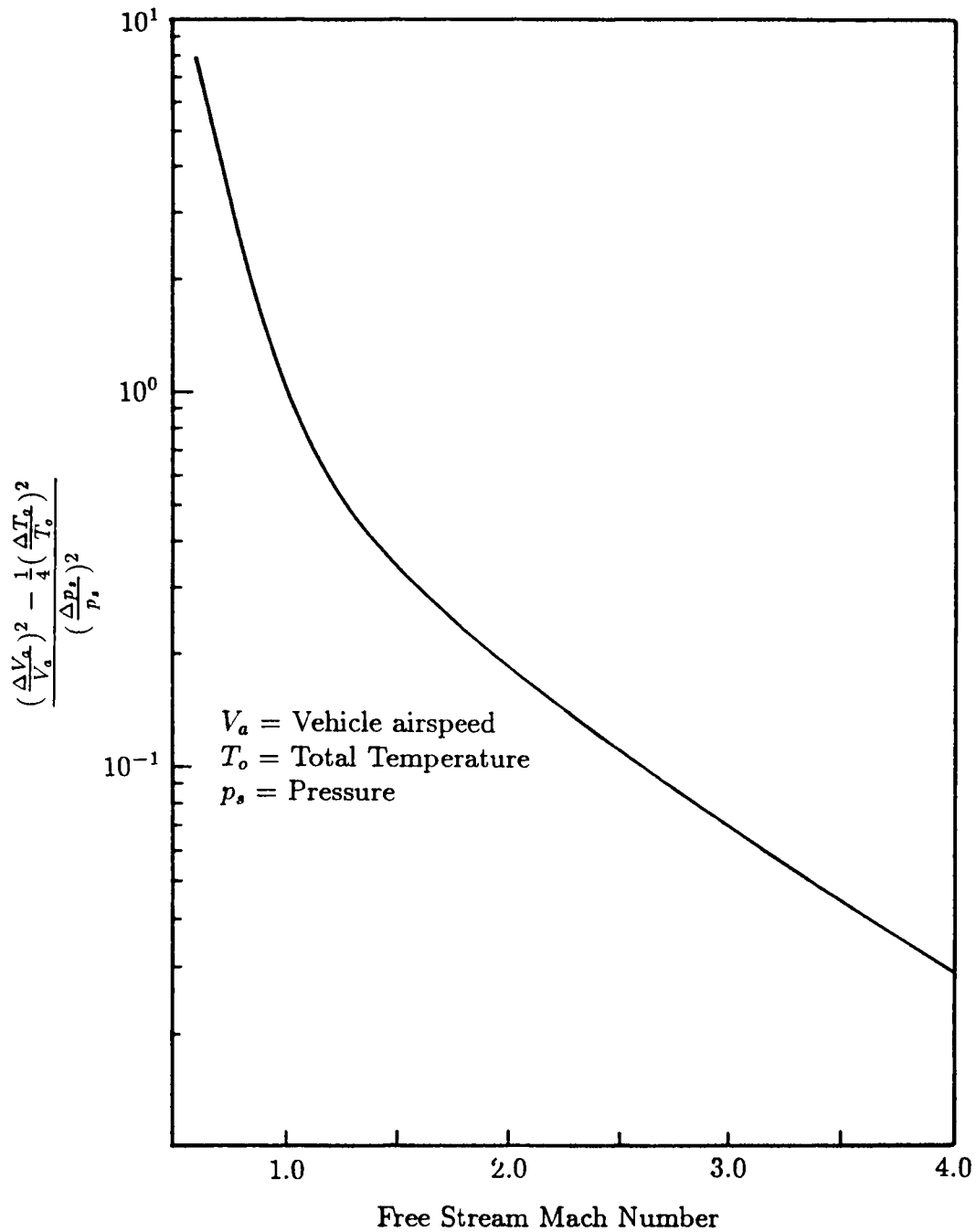


**Figure 4.3 Calculated Airspeed Uncertainty from Pressure and Temperature Measurement Uncertainties.**

## Chapter V

### Rocket Performance

Orbital Sciences Corporation (OSC), a sole source for meteorological sounding rockets, was consulted for information regarding the availability of small rockets suitable for carrying an instrumentation payload for measurements used for wind velocity calculations. Two options were discussed with OSC: 1) using an off-the-shelf, high-acceleration, high-speed meteorological rocket, and 2) designing a new rocket with low acceleration and a subsonic or low supersonic ascent rate. Present meteorological rockets are designed to deliver a payload as quickly as possible to a high altitude, which may not be suitable for the nature of the measurements needed for wind calculations.

#### Existing Design

A rocket typical of the current generation of small meteorological rockets, a Super Loki, was discussed with the OSC as potentially carrying the instrumentation pallet. In usual operations, the four-inch diameter Super Loki is used to accelerate a two-inch diameter dart to high supersonic speeds which can propel the dart to 300 kft. Though the rocket has only a two second action time, the rocket impulse imparts sufficient momentum to a low-drag dart to propel it to high altitudes. A computer simulation was conducted by OSC, assuming the instrumentation-housing cone to be no more than three inches in diameter and to weigh 30 pounds. The simulation predicted that the Super Loki would have an acceleration of 50 *g* at ignition, and 90 *g* near burnout. At burnout, the rocket would have a flight Mach number near 3.5. At 60 kft, the flight Mach number of the cone would be near 2.5. The Super Loki also has a minimum spin rate of 16

rps for stabilization.

The Super Loki is a proven rocket and is readily available. No developmental work will be necessary before the Super Loki can be used for the instrumentation pallet. Furthermore, the three-inch diameter dart design facilitates the use of existing Super Loki launchers, which are available at Kennedy Space Center and other launch sites. However, the Super Loki has two characteristics which make it undesirable as a platform for measurements pertinent to wind velocity calculations: high acceleration and high airspeed.

The predicted Mach number of a dart propelled by the Super Loki is shown in Figure 5.1. The high acceleration of the Super Loki induces a maximum

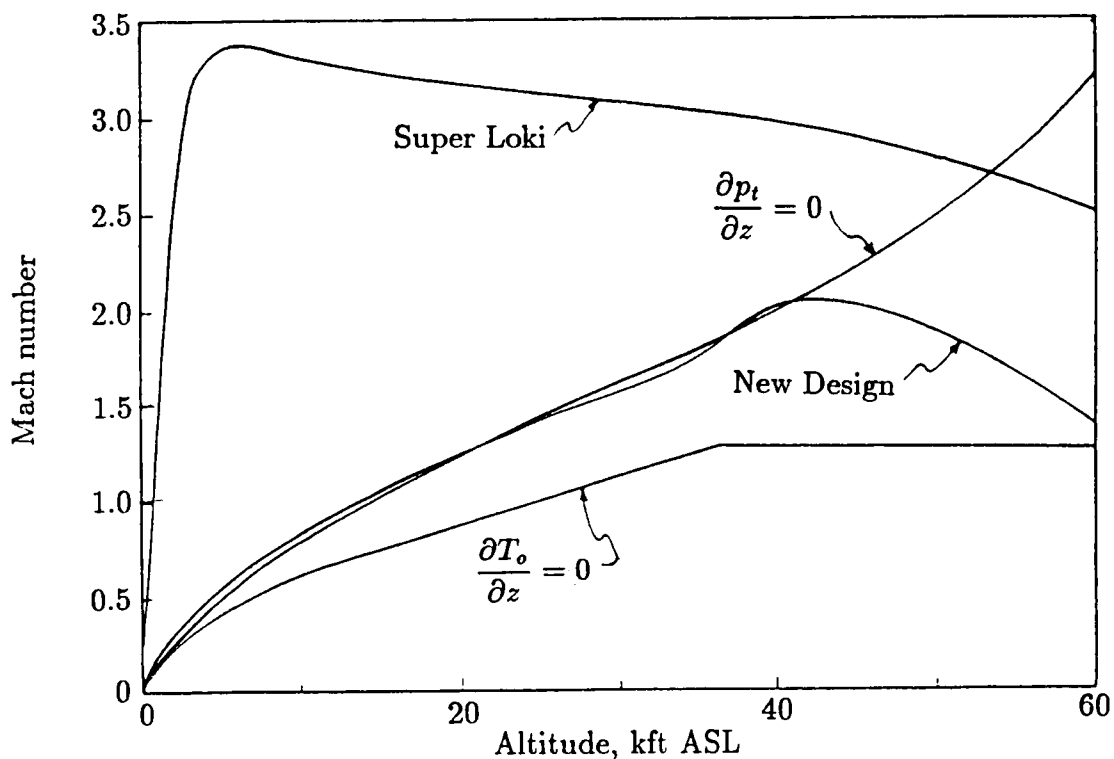


Figure 5.1 Super Loki and New Design Predicted Mach Number with a 30-pound, 3-inch Diameter Dart.

airspeed of 3900 fps at a low altitude. This acceleration typically induces errors in the transducers in the dart which may not be correctable without extensive testing and calibration. Additionally, the high airspeed requires that the pitot and temperature measurements be made more accurately than would be necessary at a lower airspeed for equivalent wind vector accuracies. Thus, OSC made a preliminary design of a rocket specifically intended for the proposed instrumentation pallet for wind velocity calculations.

### New Design

A rocket specifically designed for delivering an instrumentation pallet to 60 kft ASL would ideally have a low acceleration and a flight Mach number which increases steadily with altitude. The low acceleration provides two advantages with respect to the instrumentation: 1) the instrumentation selection would not be limited to models especially designed to withstand high g forces, and 2) a steadily increasing flight Mach number would be advantageous with respect to the total pressure and total temperature to be measured from the rocket probe.

OSC proposed the design and construction of a new, low acceleration rocket for the wind measurement platform. The proposed rocket was conceptualized as an end-burning rocket with a 7-inch diameter and a length of 48 inches. Since present-day solid propellants are designed to burn quickly, a slower burning "old" technology propellant would be used. The spin rate of the proposed rocket would be determined only after a test flight; afterwards, the fins of the rocket could be canted to adjust the spin rate. Because of the slower speed and higher moment of inertia of the proposed rocket, the proposed rocket would have a spin rate less than that of the Super Loki.

OSC simulated such a rocket ascending with the instrumentation pallet for

wind measurements. The simulation predicted that the rocket would ascend with a typical acceleration of 2 g, achieving sonic velocity at 10 kft ASL. The maximum Mach number predicted was 2.1, which occurred at rocket burnout near 50 kft ASL. The predicted Mach number of a dart propelled by the proposed rocket is shown in Figure 5.1.

The simulation of a Super Loki predicted that the total pressure behind the bow shock of the air data probe will be 190 psia at 5000 ft ASL, the altitude of maximum Mach number. At 60 kft ASL, when the dart begins coasting near Mach 2.5, the total pressure decreases to 10 psia. The wide range of total pressures potentially encountered by a dart on a Super Loki dictates that two or more pressure transducers are necessary for the precision requirements of the wind calculation since this range spans nearly three orders of magnitude. However, a dart with a Mach number that increases with altitude will generally experience a total pressure with far less variation, thus simplifying the total pressure measurements. The flight Mach number necessary for an ascending dart to maintain a constant total pressure behind a normal shock is shown in Figure 5.1 for a standard day ambient pressure profile [24]. Also shown for reference is the necessary Mach number to maintain a constant total temperature with a standard day temperature profile.

Figures 5.2 and 5.3 show the predicted total pressures and total temperatures, respectively, potentially encountered by the dart propelled by a Super Loki and the proposed rocket. The static pressures encountered by both should range between approximately 15 psia at sea level and 1 psia at 60 kft, depending on the location of the static pressure tap on the dart. The low variation in the pitot and temperature measurements, as well as the acceleration measurements, for the proposed rocket makes a broader range of transducers available with accuracies necessary for high quality wind vector calculations. This makes the transducer selection easier and



less expensive than if the Super Loki is used. However, the proposed rocket is not currently available and would have to be developed.

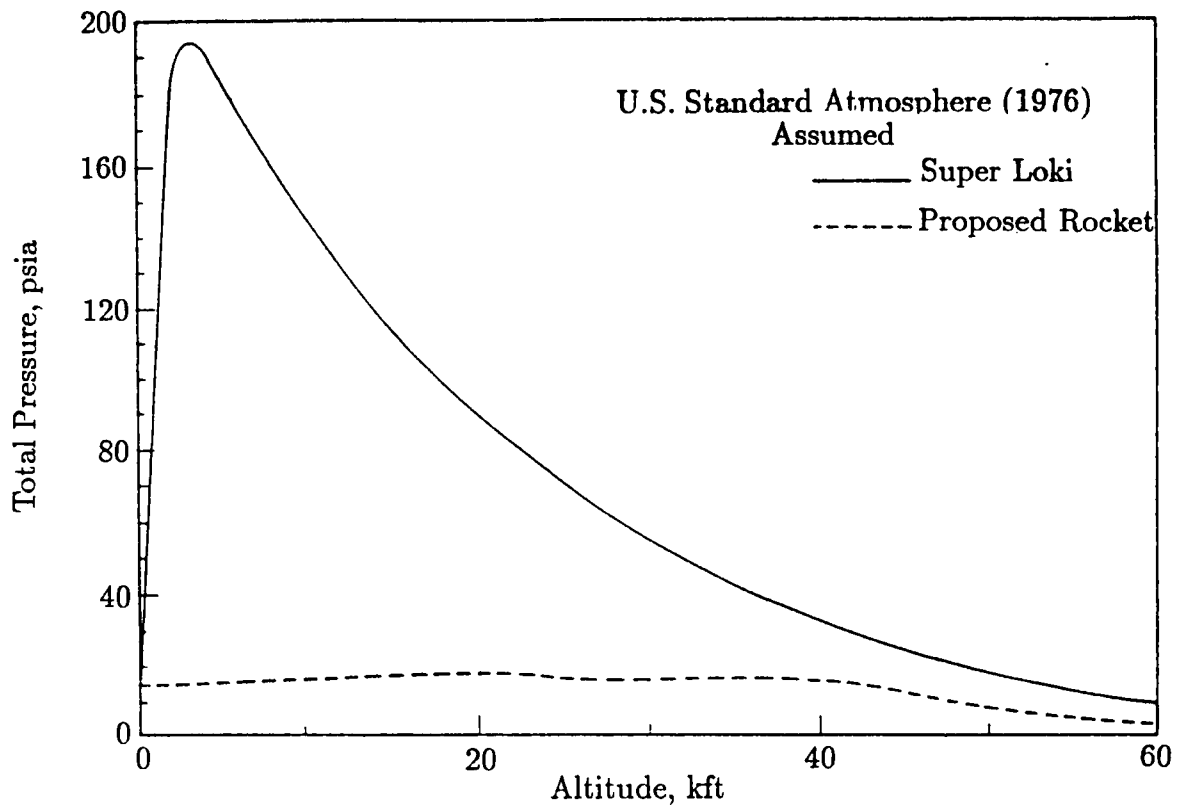
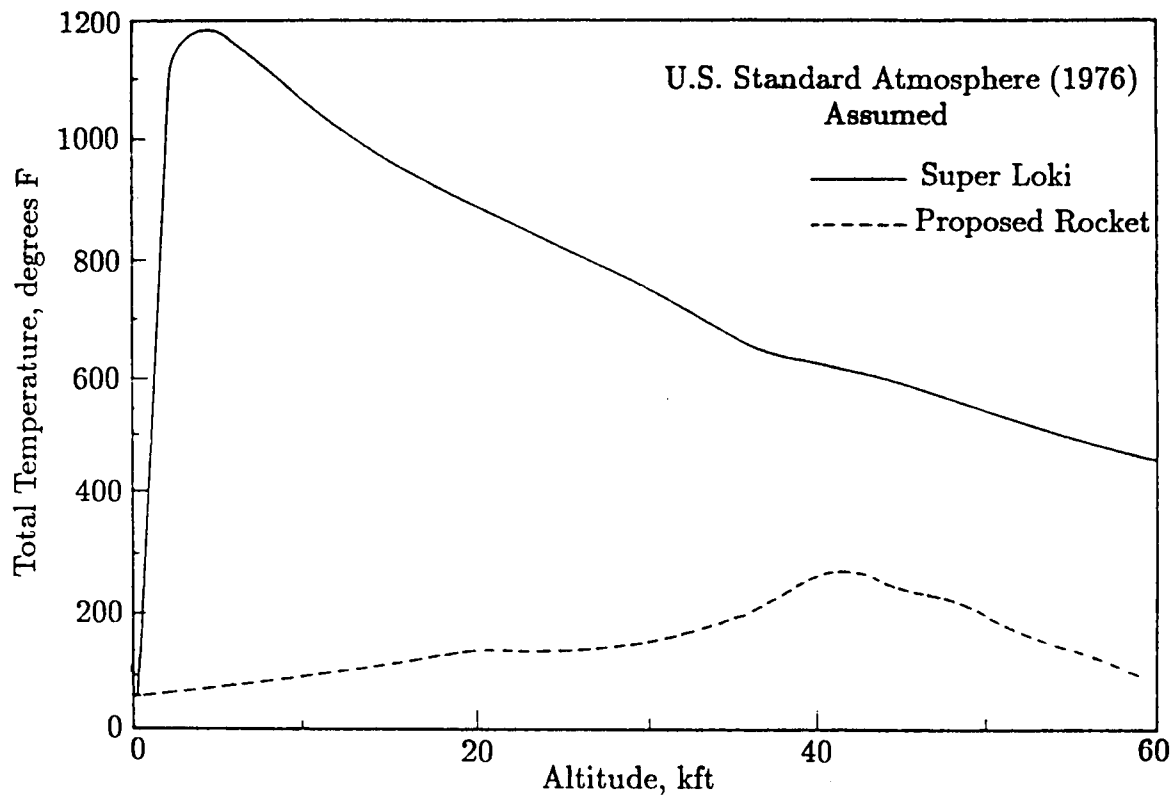


Figure 5.2 Predicted Total Pressure for a 30-pound, 3-inch Diameter Dart.



**Figure 5.3 Predicted Total Temperature for a 30-pound, 3-inch Diameter Dart.**

## Chapter VI

### Instrumentation Specification and Wind Velocity Uncertainty

The uncertainty of the calculated wind velocity from measurements made on the Dryden F-104 airplane will be used as a design specification for the instrumentation on the rocket-borne pallet. The F-104 airplane was instrumented specifically for the study of using airplanes to support shuttle launches and flies supersonically at high altitudes (above 30 kft ASL), as is expected of the rocket-borne pallet. The high altitude Mach number of the F-104 airplane is typically 1.6 to 2.0. Given the limit on the wind velocity uncertainty, the maximum measurement uncertainty can be specified.

A wind speed uncertainty of 10 fps will be used as the RMS of the wind velocity component uncertainties of the calculations from the data gathered from the F-104 airplane. The uncertainty of the wind velocity calculations from the data gathered from the F-104 airplane will be deduced from Haering [23] and Luers [2]. Haering [23] reports a wind speed uncertainty of 10 fps in supersonic flight, neglecting the errors in the measurement of the inertial velocity of the F-104 airplane. The inertial speed uncertainty of the F-104 airplane will be assumed to be 2 fps, based on the uncertainty in the wind speed calculated from the radar tracking data of Jimsphere trajectories [2]. Because the uncertainty of the Jimsphere winds of 2 fps is actually the uncertainty in the horizontal speed of the Jimsphere, this uncertainty will be used as the uncertainty of the inertial speed of the F-104 airplane. The wind velocity uncertainty of 10 fps is then derived by substituting the wind speed uncertainty of 10 fps (which ignores inertial velocity uncertainties) and an inertial velocity uncertainty of 2 fps into Equation (4.2).

### Maximum Measurement Uncertainty for Design

The uncertainty in the wind velocity calculation is directly related to the airspeed of the vehicle, as shown in part by Figure 4.3. This is also readily realized by Equation (4.28) and (4.33), which show that even for small errors in flow angle measurements, the inertial attitude measurements, the vehicle acceleration measurements, and the relative air speed measurement, a high airspeed will drive a large uncertainty in the wind velocity calculation. Thus, for the purposes of the analysis, the highest nominal airspeed anticipated from the candidate rockets will be used for instrument specifications. For the Super Loki and the proposed rocket, nominal maximum airspeeds of 3900 fps and 2200 fps will be used, respectively, based on the predicted flight Mach numbers of these rockets shown in Figure 5.1. Additionally, because of the dependence of the ground velocity calculation on the time from launch, an airspeed of 2800 fps will be studied for the Super Loki. The airspeed of 2800 fps is the predicted airspeed of the Super Loki at 60 kft ASL, after a 20 second flight. The same analysis will not be done for the proposed rocket, since the maximum airspeed is predicted to occur near 50 kft ASL, near the end of the predicted flight of the proposed rocket (one minute after launch).

Table 6.1 shows the maximum measurement error allowed for the each of the transducers to attain a wind velocity uncertainty of 10 fps, assuming each of the transducers was considered without regard to the measurement error of the other transducers. This first approximation of the measurement accuracy requirements establishes an instrumentation specification baseline, with each of the measurement errors contributing roughly equally to the wind velocity uncertainty. The wind velocity uncertainties resulting from the combined measurement errors are also given in Table 6.1. The wind velocity uncertainties resulting from the combined measurement errors are approximately twice the established design

**Table 6.1 Baseline Instrumentation Specification.**

	Proposed Rocket	Super Loki	Super Loki
Mach number	2	3.5	2.5
t, sec	54	2	20
$\Delta p/p, \%$	1.0	1.2	1.0
$\Delta T/T, \%$	0.9	0.5	0.7
$\Delta \alpha, \text{deg}$	0.2	0.1	0.1
$\Delta \phi, \text{deg}$	0.1	0.07	0.1
$\Delta a, \text{milli-g}$	6	200	20
Wind Velocity Uncertainty, fps	22	23	22

uncertainty of 10 fps.

As a second approximation to the maximum measurement errors allowed, the measurement uncertainties shown in Table 6.1 were halved. The resulting wind velocity uncertainties were half of those given in Table 6.1, implying that the wind velocity uncertainty is directly proportional to the measurement errors within the neighborhood of the measurement errors listed in Table 6.1. The resulting wind velocity uncertainties, 11 fps for the Super Loki and 12 fps for the proposed rocket, are considered equivalent to the uncertainty of the wind speed calculations from the F-104 based measurements.

Transducers with measurement uncertainties which will meet or exceed the requirements established for the pressure, temperature, and acceleration measurements for the two different rockets are commercially available, but may be cost prohibitive. The measurement accuracy requirements of the flow angles,  $\alpha$  and  $\beta$ , however, probably cannot be met for the high speed Super Loki.

#### Pressure and Temperature Measurement Feasibility

Rosemount pressure and temperature transducers were chosen as typical of commercially available aerospace transducers. Rosemount sells capacitive pressure transducers with a 0.1% full scale accuracy [25] and total temperature probes with a 0.2% scale accuracy [26]. The Rosemount pressure transducers would readily meet both the total and static pressure requirements of both rockets. Both rockets would require two transducers, for low and high ranges, for both the total and static pressures measurements.

The temperatures induced by the high Mach numbers of the Super Loki would be difficult to measure. The Rosemount strut-mounted temperature probes have maximum temperature ranges typically of 600°F, which is inadequate for the Su-

per Loki but adequate for the proposed rocket. The accuracy of the Rosemount temperature probes will also meet the measurement requirements of the proposed rocket. The temperatures induced by the high Mach numbers of the Super Loki would probably require a custom-made RTD probe to cover the required range and meet the temperature measurement accuracy requirements.

#### Inertial Attitude Measurement Feasibility

The inertial attitude measurement uncertainty cannot be quantified without *a priori* knowledge of the rocket flight dynamics. The bank angle would be determined by linear accelerometers and the local gravity vector. This accuracy is assumed herein to be 0.1 deg, based on the resolution of a 12 bit analog to digital (A/D) transducer signal conversion. The dynamics of the rocket on the off-centerline axes will be driven by aerodynamic side loading, which is expected to be small because of the high airspeed of either rocket. Potentially, the only error in the angular rate transducer signals will be linearity errors, which will be small due to the small angular motions of the rocket off of the centerline. Furthermore, linearity errors should tend to cancel because the spin of the rocket brings the rate transducers into a given plane twice, with opposing orientations, with each revolution of the rocket. Thus, the attitude uncertainty on the off-centerline axes will be assumed to be 0.1 deg, modeled after the attitude uncertainty of the ER-2 MMS and the F-104 based measurements, both of which use strap-down INSs for attitude measurements. This uncertainty is not adequate for the Super Loki but is adequate for the proposed rocket.

#### Acceleration Measurement Feasibility

The acceleration measurement range and accuracy requirements of both rockets can be met with commercially available accelerometers. Schaevitz accelerom-

eters [27], one with a full range of  $\pm 5$  g on the body-fixed x-axis, and two with full ranges of  $\pm 0.5$  g on the body-fixed y- and z-axes, will satisfy the acceleration measurement range anticipated with the proposed rocket. These accelerometers have an accuracy of  $3.5 \times 10^{-3}$  g and  $0.4 \times 10^{-3}$  g accuracy, respectively. The Super Loki acceleration on the body-fixed x-axis would be measured by a Sunstrand accelerometer [28] with a range of  $\pm 100$  g and an accuracy of  $10 \times 10^{-3}$  g. The Super Loki acceleration on the body-fixed y- and z-axes would be measured by the same low range Schaevitz accelerometers potentially used on the proposed rocket.

#### Flow Angle Measurement Feasibility

The uncertainty of the flow angle measurements is driven more by the calibration of the flow angle probe than by the accuracy of the differential pressure transducer supporting the measurement. The flow angles are anticipated to be small, because of both the anticipated high air speed of the rockets (compared to the side loading from the wind) and because of the rockets' natural tendency to seek a zero angle of attack and sideslip angle, nullifying side loading. Even an extreme wind of 200 fps above KSC [29] would result in a flow angle of less than 6 deg or less for the high speed rockets. However, this angle would have to be considered as superimposed on the rocket angle of attack due to coning. Thus, the requirements on the accuracy of and range of the differential pressure transducers can be easily met with a bi-directional differential pressure transducer with an appropriate range of  $\pm 2.5$  psid, based on the factory calibration of the Rosemount 858AJ hemispherical flow direction probe [16].

The accuracy of the data taken from the probe will be assumed to be limited to 0.1 deg. This is the accuracy claimed by Rosemount [20] with correction for port misalignment, and this accuracy is not inconsistent with the findings of other



researchers [17, 18, 21, 22], as discussed in Chapter III. Further resolution on the flow angle measurement may be restricted by boundary layer turbulence or the finite surface area required by the orifice for the pressure measurement.

A flow angle accuracy measurement of 0.1 deg is inadequate for the Super Loki but is adequate for the proposed rocket. Although flow angle measurements are made with an accuracy of 0.03 deg by the ER-2 MMS [15], this accuracy apparently cannot be attained by a small differential pressure probe. The ER-2 MMS uses differential pressure measurements across the large radome of the ER-2, which has been carefully studied in wind tunnels. Conceivably, a nose cone can be designed and carefully calibrated for a dart propelled by the Super Loki with a high flow angle sensitivity in the Mach number range predominant in the predicted Super Loki flight (2.5 - 3.5). This, however, is beyond the scope of this thesis.

#### Rocket and Measurement Specifications

Based on the preceding analysis of instrumentation availability and measurement accuracies, the development of the proposed rocket is recommended as a platform for measurements for wind profile calculations. Because of the high air-speed of the Super Loki and the limitations on the accuracy of the flow angle and the attitude measurements, the uncertainty of the wind velocity calculations from measurements made from the Super Loki will be high compared to that from the proposed rocket.

Table 6.2 lists the potential measurement accuracy of commercially available transducers, propelled by the proposed rocket, and the resulting uncertainty in the final wind velocity calculation. Although the resulting uncertainty is higher than the design uncertainty from the F-104 based measurements, it is competitive with the F-104. This uncertainty is also based on the maximum predicted airspeed and

the selection of instrumentation based on the predicted conditions at the maximum airspeed.

The measurement uncertainties listed in Table 6.2 are presented as transducer errors. However, the transducers are only part of a system which is comprised also of signal conditioning, multiplexing, analog to digital (A/D) signal conversion, and telemetry electronics. Thus, the dart as a system would have to be calibrated in the laboratory for bias and linearity errors. Once on the launch pad, a data point for ambient conditions would be recorded to partially determine system "drift" from storage, handling, temperature, and other effects.

**Table 6.2 Final Instrumentation Specification.**

	Proposed Rocket
Mach number	2
t, sec	54
$\Delta p/p, \%$	0.5
$\Delta T/T, \%$	0.5
$\Delta \alpha, \text{deg}$	0.1
$\Delta \phi, \text{deg}$	0.1
$\Delta a, \text{milli} - g$	3.5
Wind Velocity Uncertainty, fps	13

## Chapter VII

### Conclusions

An instrumentation pallet, carried by a meteorological rocket, can be built with off-the-shelf transducers to make measurements for wind velocity calculations with accuracies comparable to calculated wind velocities from airplane measurements. The dart housing the transducers and supporting data acquisition electronics would have to be propelled by a relatively low speed, low acceleration rocket, which would have to be developed.

The potential instrumentation pallet studied herein is modeled after the pallets on research airplanes which report wind velocities. The air velocity relative to the vehicle is transformed by the attitude and motion of the vehicle to the frame of an observer on earth. However, because of the high air speed of a rocket, the pressure and temperature measurements must have low uncertainties, less than 1%, to produce calculated wind velocities with the same confidence as the transducers on a slower airplane. The flow angles and Euler angles must be accurate to within 0.1 deg, and the acceleration measurements of the rocket and dart must be accurate to within a few milli-g.

The motors typically used for meteorological soundings are characterized by high acceleration and high airspeeds, both of which are unsuitable for the measurements supporting wind velocity calculations. Thus, a slower rocket is recommended to support these measurements.

The simplicity and performance of the rocket make that system more desirable for supporting space vehicle launches than existing measurement systems. A rocket can traverse the space of interest and collect the information for the wind velocity

calculation in less than one minute, whereas the presently-used balloons require one hour and radar support.

A significant finding in the research for this work was the absence of an explicitly defined minimum wind measurement uncertainty for space vehicle launch support. Because significant interest does exist to find an alternative wind measurement tool to the Jimsphere/radar system currently in use, a wind measurement standard should be established. This standard could easily be the Jimsphere/radar system, since it is not the accuracy of the this system which is undesirable, but the time required to make the wind profile measurement.

LIST OF REFERENCES

## LIST OF REFERENCES

1. Paige, T.S., A.E. Nelius, P.J. Murphy, and W. Frost. "Instrumented Rocket Wind Profiler." final report to NASA Marshall Space Flight Center for SBIR contract NAS8-38465, August, 1990.
2. Luers, J.K., and C.D. MacArthur. "Ultimate Wind Sensing Capabilities of the Jimsphere and Other Rising Balloon Systems." NASA CR-2048, June, 1972.
3. Bell, T.E. "Wind shear cited as likely factor in shuttle disaster." The Institute. May, 1987.
4. Bjarke, L.J., and L.J. Ehernberger. "An In-Flight Technique for Wind Measurement in Support of the Space Shuttle Program." NASA TM 4154, November, 1989.
5. Hatley, C.M. "Prelaunch Wind Monitoring Via Aircraft." CR S33450D, SIR Presentation at Johnson Space Center, Houston, Texas, November 14, 1989.
6. Etkin, B. Dynamics of Atmospheric Flight. New York: John Wiley & Sons, 1972.
7. Shapiro, A. H. The Dynamics and Thermodynamics of Compressible Fluid Flow. New York: The Ronald Press Company, 1953.
8. Howarth, L., H.B. Squire, and C.N.H. Lock, eds. Modern Developments in Fluid Dynamics High Speed Flow Vol. II. Great Britain: Oxford at the Clarendon Press, 1956.
9. Volluz, R.J. "Handbook of Supersonic Aerodynamics, Section 20, Wind Tunnel Instrumentation and Operation." NAVARD Report 1488 (Vol. 6), January 1961.
10. Lenschow, D.H. "Aircraft Measurements in the Boundary Layer." Probing the Atmospheric Boundary Layer. Boston: American Meteorological Society, D.H. Lenschow, ed., 1986.
11. Chue, S.H. "Pressure Probes for Fluid Measurement." Progress in Aerospace Sciences. Vol. 16, No. 2, pp. 147-223, 1975.
12. Gracey, W. Measurement of Aircraft Speed and Altitude. New York: John Wiley & Sons, 1981.

13. Vahl, W.A., and R.L. Weirich. "Calibration of 30° Included-Angle Cone for Determining Local Flow Conditions in Mach Number Range of 1.51 to 3.51." NASA TN D-4679, August, 1968.
14. Brown, D.L. "Predicting Equilibrium Pressures from Transient Pressure Data." ARL 65-7, January, 1965.
15. Scott, S.G., T.P. Bui, K.R. Chan, and S.W. Bowen. "The Meteorological Measurement System on the NASA ER-2 Aircraft." Ames Research Center, Revised June, 1989.
16. "Rosemount Model 858 Flow Angle Sensors." Rosemount, Inc., Bulletin 1014, 1988
17. Dudzinski, T.J., and L.N. Krause. "Flow-Direction Measurement with Fixed-Position Probes." NASA TM X-1904, October, 1969.
18. Gaillard, R. "Calibration and Use of an ONERA Miniature Five Hole Probe." Office D'Etudes et de Recherches A'erospatiales, September, 1983.
19. Bryer, D. W., and R.C. Pankhurst. Pressure-probe Methods for Determining Wind Speed and Flow Direction. London: Her Majesty's Stationary Office, 1971.
20. Hagen, F. W., Rosemount, Inc., Aerospace Division, conversation with T.S. Paige, May, 1990
21. Brown, E., National Center for Atmospheric Research, conversation with T. S. Paige, July, 1990.
22. Poellet, M., University of North Dakota, conversation with T. S. Paige, July, 1990.
23. Haering, E.H. "Airdata Calibration of a High-Performance Aircraft for Measuring Atmospheric Wind Profiles." NASA TM 101714, January, 1990.
24. U.S. Standard Atmosphere, 1976 NOAA-S/T 76-1562, 1976
25. "Series 1332/1333 General Purpose Capacitive-Type Pressure Transducers." Rosemount, Inc., Product Data Sheet 2200, 1983.
26. "Total Temperature Sensors." Rosemount, Inc., Bulletin 1012, 1989.

27. "Linear and Angular Servo Accelerometers." Schaevitz Technical Bulletin 4501F, 1988.
28. "Model 2181 Mini-Pal Servo Accelerometer." Sunstrand Data Control, Inc., 1990.
29. Turner, R. E., and C.K. Hill, "Terrestrial Environment (Climatic) Criteria Guidelines for Use in Aerospace Vehicle Development, 1982 Revision." NASA TM 82473, June, 1982.
30. Panton, R.L. Incompressible Flow. New York: John Wiley and Sons, 1984.
31. Sakamoto, G.M. "Aerodynamic Characteristics of a Vane Flow Angularity Sensor System Capable of Measuring Flightpath Accelerations for the Mach Number Range from 0.40 to 2.54." NASA TN D-8242, May, 1976.



APPENDIX

## Appendix

### Transformation of a Vector in a Rotating Coordinate System with Angular Rate Measurements

Etkin [6] derives the transformation of a vector in a coordinate frame to a reference coordinate frame in the context of an airplane (the rotated coordinate system) and the earth (the inertial, or reference coordinate system). The rotating frame, or body-fixed frame, is rotated through a series of one dimensional rotations in a fixed sequence:  $\psi$ ,  $\theta$ , and  $\phi$ , which correspond to the airplane heading, elevation, and bank angles. These angles would be determined by free gyroscopes or calculated from rate gyroscope measurements in the airplane inertial navigation system (INS) for wind velocity calculations. However, if rate gyroscopes or angular rate sensors are used in place of an INS on the rocket, the rocket attitude must be determined by integration of the three dimensional rotation rate of the rocket measured in the body-fixed frame.

A discrete rotation, measured in the body-fixed frame rate gyroscopes or angular rate sensors, is realized by a transformation of the Eq. (2.14). Panton [30] transforms a vector into a rotated frame by defining the components of the vector in the rotated frame as the inner product of the vector in the fixed frame and the unit vectors describing the axes of the rotated frame. Using index notation, the components of a vector in a rotated frame are described by

$$x'_i = \vec{V} \cdot \vec{x}'_i \quad (A - 1)$$

where  $x'_i$  is the  $i^{th}$  component of the vector in the rotated frame,  $\vec{V}$  is the vector in the fixed frame, and  $\vec{x}'_i$  is the unit vector in the fixed frame lying on the  $i^{th}$  axis of

the rotated frame. Combining Pantón's [30] presentation and Etkin's [6] approach to the vector transformation, the rows of the transformation matrix, Eq. (2.13), are recognized as unit vectors on the axes of the body-fixed coordinate system.

The unit vectors lying on the axes of the rotated frame can be broken into two components, based on the measured rotation vector, as shown in Figure A-1. The first of the two components,  $\vec{F}$ , which is fixed through the rotations, is added to a vector  $\vec{R}'$ , which rotates in a plane orthogonal to  $\vec{F}$ .  $\vec{F}$  is the projection of the rotating coordinate axis on the rotation axis,  $\vec{\omega}$ .  $\vec{R}$  is the vector difference between the unrotated axis,  $\vec{x}_i$ , and  $\vec{F}$ :

$$\begin{aligned}\vec{R} &= \vec{x}_i - \vec{F} \\ &= \vec{x}_i - \frac{\vec{\omega}}{\omega^2}(\vec{x}_i \cdot \vec{\omega})\end{aligned}\tag{A-2}$$

As the coordinate frame rotates, and the axis  $\vec{x}_i$  rotates into  $\vec{x}'_i$ ,  $\vec{F}$  remains fixed and  $\vec{R}$  rotates into  $\vec{R}'$ . The solution of  $\vec{R}'$  thus leads directly to the determination of the direction of the new axis through Eq. (A-2)

$\vec{R}'$  rotates in a plane orthogonal to  $\vec{\omega}$  by the magnitude  $\omega\Delta t$ . Since  $\vec{R}'$  is orthogonal to  $\vec{\omega}$ , the inner product of  $\vec{\omega}$  and  $\vec{R}'$  is zero:

$$\vec{\omega} \cdot \vec{R}' = 0\tag{A-3}$$

The angle between  $\vec{R}$  and  $\vec{R}'$  is known by  $\omega\Delta t$ . Thus

$$\vec{R} \cdot \vec{R}' = R^2 \cos(\omega\Delta t)\tag{A-4}$$

A third relation for  $\vec{R}'$  can be found from the vector cross product of  $\vec{\omega}$  and  $\vec{R}$ , which is a vector orthogonal to both of these vectors. Furthermore, the angle between  $\vec{\omega} \times \vec{R}$  and  $\vec{R}'$  is readily seen from Figure A-1 as  $\frac{\pi}{2} - \omega\Delta t$ . Thus

$$\begin{aligned}\vec{\omega} \times \vec{R} \cdot \vec{R}' &= R |\vec{\omega} \times \vec{R}| \cos\left(\frac{\pi}{2} - \omega\Delta t\right) \\ &= \omega R^2 \sin \theta\end{aligned}\tag{A-5}$$

Eq. (A-3), (A-4), and (A-5) can be solved simultaneously for the components of  $\vec{R}'$ . The direction of the new axis, referenced to the fixed frame, is then

$$\vec{x}'_i = \vec{F} + \vec{R}'\tag{A-6}$$

which is substituted as the  $i^{\text{th}}$  row in the transformation matrix defined by Eq. (2.14). This process is repeated for all three coordinate axes.

- $\vec{\omega}$  = Rotation Rate Vector
- $\vec{x}_i$  =  $i^{\text{th}}$  Coordinate Axis
- $\vec{x}'_i$  = Rotated  $i^{\text{th}}$  Coordinate Axis
- $\vec{F}$  = Fixed Vector
- $\vec{R}$  = Initial Rotating Vector
- $\vec{R}'$  = Final Rotating Vector

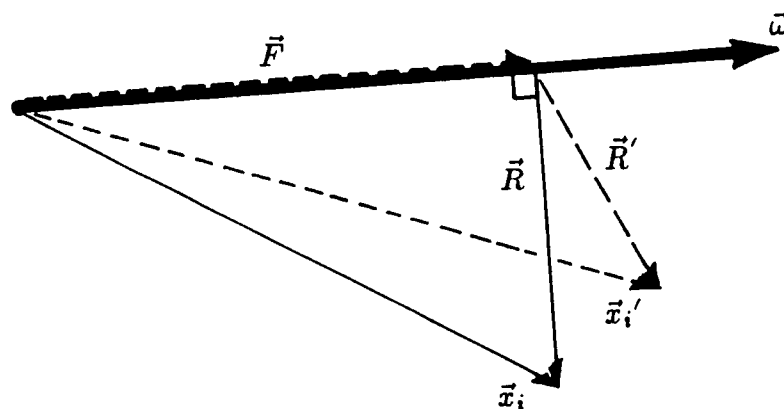
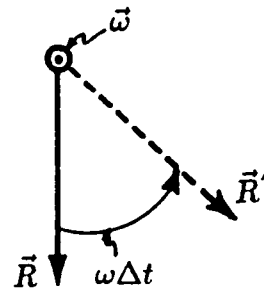


Figure A.1 Decomposition of a Rotating Coordinate Axis into Fixed and Rotating Components.

## VITA

Terry S. Paige was born in Millington, Tennessee, on January 18, 1964. He graduated from The University of Tennessee at Chattanooga in 1986. While attending school in Chattanooga, he married Ellen Ann Edwards of Chattanooga and worked as an engineering aide with the Tennessee Valley Authority.

After graduating, he worked for Sverdrup Technology, Inc., at Arnold Engineering Development Center in the Engine Test Facility. He currently works for FWG Associates, Inc., in Tullahoma, Tennessee, and is attending graduate school at the University of Tennessee Space Institute.

Mr. Paige lives in Cowan, Tennessee, with his wife and children, Patrick Steven and Audrey Lynn, three cats and four fish.